平成７年度 学位請求論文

Study on Widely Tunable Distributed Forward- and Backward-Coupling Semiconductor Laser Diodes

（広帯域波長可変分布並進逆進結合型半導体
レーザダイオードに関する研究）

Author

SATO Kenji

佐藤　健二

Student No. 37106

Department of Electronic Engineering

Faculty of Engineering

University of Tokyo

東京大学 大学院

工学系研究科 電子工学専攻

Research Advisor

Professor Dr. TADA Kunio

多田 邦雄　教授

平成７年 12 月 20 日提出

Contents

Chapter 1 Introduction

1.1 Research Background

Distributed Feedback (DFB) semiconductor lasers have been making remarkable progress of performance and the number of their applications has become extremely large. Since Kogelnik and Shank studied DFB lasers (both index and gain coupled) in 1972 [1-1], a considerable number of researchers have been tried to realize the higher performance of DFB semiconductor lasers. DFB lasers have been applied for advanced optical communication systems, optical measurement equipments, optical integrated circuits, optical computing, and they are required to have excellent single longitudinal mode properties [1-2], high yield, immunity to facet reflection, resistance to external optical feedback, wider bandwidth, and narrow linewidth. More and more researchers have been recently studying about gain-coupled(GC)-DFB lasers because their excellent features would be suitable for advanced communication systems. The biggest advantage of GC-DFB lasers is the mode stability [1-3], however it implies that GC-DFB lasers would not be tuned easily. There have never existed tunable GC-DFB lasers because of the strong mode stability. However GC-DFB lasers would be a better tunable light source because the mode stability would be also required once one of the channels is selected. In this doctor's thesis we propose a new type of widely tunable DFB semiconductor lasers --- distributed forward- and backward-coupling lasers -- which would provide more than 40 nm tuning range for 1.55 μm wavelength scheme. It would provide a wide tuning range (over 40 nm, for example) as well as larger SMSR in principle compared with the other types of discontinuously-tunable laser diodes. Simple one current tuning scheme is another advantage of the DFBC laser. Either gain or index coupling, or a combination of these may be used with the DFBC laser. However, the gain coupling is preferable

as it could lead to larger SMSR.

In this introductory chapter we give a brief overview of the history of DFB lasers and we show the advantage of gain-coupled DFB lasers. Then the purpose and contents of this thesis are described.

1.1.1 Index-Coupled and Gain-Coupled DFB Laser

The stimulated emission of photons by the recombination of carriers injected across a p-n junction can make an optical waveguide the amplifying medium. In order to realize the lasing oscillation, feedback must exist inside the resonator. In the early time of research activities of semiconductor lasers, the most common way was to place mirrors at the two ends of the cavity. The most simple way was to make both facets cleaved which provide reflection. Such a structure is generally called the Fabry-Perot cavity. In order for positive feedback to occur, the forward-going wave must be in phase with the backward wave. However the relatively wide bandwidth of the gain spectrum of semiconductor insures that many side modes could also gain enough power to prevent single mode oscillation [1-1].

The DFB structure provides feedback through diffractions due to periodic perturbation of the medium. Similar to the X-ray diffraction, waves traveling at one direction will be diffracted at a certain angle. For resonance to occur, the forward-going wave must be able to diffract approximately π in order to couple with the backward going wave and vice versa for positive feedback. Since feedback is distributed over the length of the grating, we thereby attach the name distributed feedback structure. And as with X-ray diffraction, the wavelength of the light inside this structure must nearly satisfy the so called Bragg condition. Analogous to the Fabry-Perot resonance condition, the length of the periodic pitches of the grating

must equal an integral number of half wavelength,

$$\lambda=\frac{2\Lambda}{M} \tag{1-1}$$

where Λ is the length of the pitch and M, an integer, denotes the order of the grating. As we can see the spectral selectivity of this structure comes from the fact that only at those wavelengths which nearly satisfy the Bragg condition would there be significant coupling of the forward and backward waves. Thus even if the gain spectrum of the active medium is represented by a flat curve, the wavelength sensitivity of the Bragg effect will limit the possibility of multi-modes oscillation.

However, there still remain many problems to this structure. For example, if we are considering the index-coupled DFB laser, whereby the perturbation comes from a periodic modulation of the refractive index, analytical studies have shown that such structures are dispersive and stop bands of frequencies exist at the Bragg frequency in which propagation is not possible. As a result, for this laser there will actually be two modes; one to the left and one to the right of the Bragg frequency with the same magnitude (mode degeneracy). Therefore we are faced with the problem of more than one mode lasing. Kogelnik and Shank also pointed out that the purely gain coupled DFB lasers can realize the only one lasing mode exactly at the Bragg frequency [1-1]. Before the story on GC DFB lasers, we show the history of improved Index-Coupled DFB lasers.

Structural changes were suggested to the fundamental index-coupled DFB laser. First of all researchers were interested in knowing whether facet reflection will alleviate or worsen the situation. After all, to eliminate reflection completely is quite difficult in real life; furthermore there will be applications such that it is more convenient to leave the facets as cleaved. As it turned out, facet reflections at both facets result in mode pulling whereby the DFB mode frequencies will approach that

of the Fabry-Perot mode. Moreover, the threshold gain of each mode will be altered according to the phase of the reflection. So while this seems like one way to eliminate mode degeneracy, the randomness of the phase of facet reflection would disable us from controlling the actual lasing mode. Selectivity is therefore lost again [1-3][1-4].

As mentioned before, the actual frequency of the lasing mode of a DFB laser without any reflection facet will deviate slightly from the Bragg frequency. As we know maximum diffraction should occur at the Bragg frequency. Therefore if somehow we can shift the oscillation frequency towards it, we should obtain a single mode at that frequency. Actually the effect of facet reflection is capable of doing that. Through mode pulling, the DFB mode can be pushed towards the Bragg mode. Unfortunately, for low coupling strength, the effect of the Fabry-Perot tends to be stronger and affects the final threshold gain of each mode.

The concept of $\lambda/4$-shifted DFB laser is subsequently evolved in solving the problem of degeneracy. A structural change is actually made in the laser in order to add an optical phase shift of $\pi/2$ to the waves traveling inside thereby allowing lasing at the Bragg frequency. Two major methods are employed to realize this phase shift: 1) phase shifting of the corrugation in an uniform waveguide; 2) phase shifting due to an nonuniform waveguide with uniform corrugations--this can be achieved by precise control in the layer thickness and/or stripe width.

Both of the above two schemes have been realized to a certain degree of success in obtaining dynamic single mode (DSM) operations. However, as one of the topic of this thesis, we will see that index-coupled DFB lasers, including those of $\lambda/4$-shifted ones, will lose its mode suppression ability when gain saturation settles in. This so-called spatial hole burning phenomenon plays a major part in causing such detrimental effects. Thus once again, we face the problem of multi-mode oscillation.

Several theories were used in explaining the exact mechanism of spatial hole burning. However the ones that have been traditionally used tend to focus on the macroscopic aspect of the problem. In our present analysis, we will attempt to look at spatial hole burning in the microscopic perspective. When we viewed under that light, we found the ideal structure in the so called gain-coupled DFB laser, which is the theme of the present thesis.

As we have mentioned earlier on, periodic perturbations can occur either to the refractive index or to the gain. In fact, it was understood in the early works on DFB lasers that the stopband in the dispersion curve which exists in the index-coupled case does not exist for the gain-coupled case. This would therefore mean that lasing is possible at the Bragg frequency given no index coupling occurs. Moreover, due to the periodic nature of the gain at this Bragg frequency, even when facet reflection exists, the locking of the gain at the primary DFB mode will negate any adverse effect of the Fabry-Perot modes. Thus, mode discrimination between the primary mode and the side modes would remain strong. This immunity to facet reflection further leads to the speculation that external reflection such as feedback from a connecting optical fiber and etc. would also have less of an effect than it would have on an index-coupled laser. This would be extremely useful in realizing efficient monolithic integrated circuits. As we will also see, the existence of this gain grating also counters the deterioration caused by spatial hole burning.

If gain-coupled DFB laser is so ideal, why has it not replaced the index-coupled laser yet? Perhaps one main obstacle lies in the difficulty in realizing the gain grating. Since any tampering with the active layer can lead to undesirable results, it was often thought that the actual fabrication of the laser would be extremely complicated. Also, it seemed that index coupling can not be avoided with the existence of gain coupling; this mixed coupling effect would mean a certain unpredictability of the properties of the laser. However, over the past six years, our

group has come up with some novel proposals in overcoming the above mentioned obstacles. Foremost of all, we have utilized a special growth kinetics of organometallic vapor phase epitaxy in order to fabricate the gain grating. In addition we have implemented two gratings whereby index coupling can be canceled due to the phase difference between the two gratings [1-5].

In 1989, the first experimental results of GC semiconductor DFB lasers were published by Y.Luo et al [1-6] (University of Tokyo, Optical Measurement Technology Development Co., Ltd., Tokyo, (OMTEC)). Since then, a number of significant contributions for the identification of several advantages and the further development of GC DFB lasers could be made and have been published by K.David (University of Gent - IMEC) [1-7]. Together with the technological improvements reported by the Univ of Tokyo, theoretical studies have attracted increasing international interest in GC DFB lasers, for example, the significant analysis of linewidth enhancement factor of GC DFB lasers by Kudo (Tokyo Inst. of Tech) [1-8] and by Lowery (University of Melbourne)[1-9]. Very recently, the experimental works have been reported, for example, B. Borchert (Siemens Research (FRG)) [1-10], W. T. Tsang (AT&T Bell Laboratories, Murray Hill) [1-11], T. Makino (AT&T Bell-Northern Research) [1-12], .

To summurize this section, several important observations were made along the way. These include 1) high yield of single mode operation[1-5], 2) facet reflection immunity[1-13], 3) less influence of optical feedback (as speculated)[1-14], 4) a much lower linewidth enhancing factor[1-9][1-15], and low-chirping short-optical-pulse generation capability[1-16]. All of these seem to indicate that an improved DFB laser has been created.

1.1.2 Tunable Semiconductor Laser

The first approaches for the realization of electronically tunable laser diodes in the 1.5 μm wavelength region concerntrated on devices with a longitudinary subdivided cavity. From the early experience, that the widest tuning range achievable with two section DFB lasers is usually limited to about one longitudinal mode spacing [1-17], research activities then focused on the development of active-passive three-section extended cavity configurations.

With DBR lasers subdivided into an amplifying, a tuning and a phase-control section (three-section DBR lasers) as shown schematically in Figure 1-1(a) tuning ranges up to 10 nm have been reported in the quasi-continuous tuning mode [1-18]. However, two different currents into the tuning and phase-control sections have to be carefully adjusted in order to obtain a smooth tuning characteristic.

Also, impressive performance in tunability and linewidth has been achieved using three-section DFB laser structures which are relatively simple to fabricate (Figure 1-1(b)). In this case, tuning results from the longitudinally nonuniform gain-phase relationship in DFB lasers [1-19], which enables the shift of the Bragg wavelength at constant total mode gain. Up to 7.2-nm continuous wavelength tuning has been demonstrated [1-20], exploiting also the thermal tuning effect. Due to the dependence of the overall cavity gain level from the carrier densities within all sections, the tuning mechanism is still more complex as compared to the three-section DBR lasers.

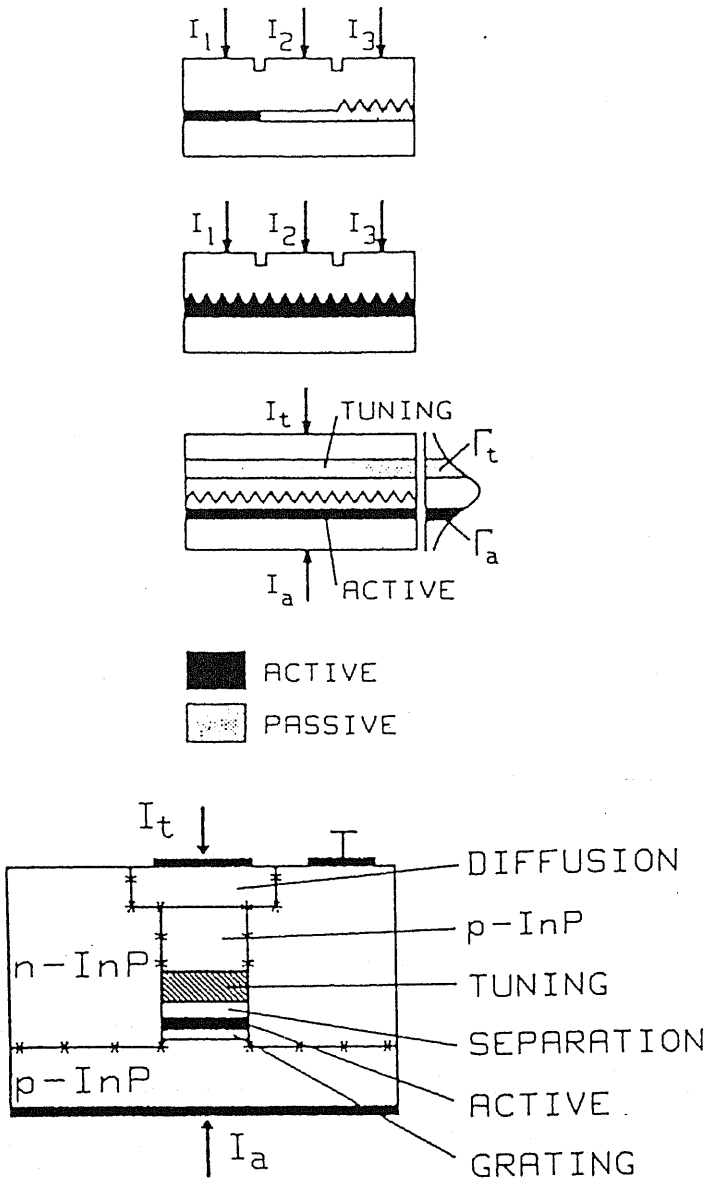

Figure 1-1 Principal longitudinal sections of (a) three-section DBR laser, (b) three-section DFB laser, (c) tunable twin-guide (TTG) laser (indicated is also the fundamental mode profile with confinement factors in the active (Γ_a) and tuning layer (Γ_t)).

In practice, the need for two or more wavelength control currents is unattractive for both manufacture and application. Only one control current should preferably be required to tune the wavelength continuously. One step towards this goal is the operation of a multisection device such that the two wavelength control currents are varied simultaneously in a fixed ratio. 3.1-nm continuous tuning has been achieved by this method [1-21]. Unfortunately, the optimum current ratio must

be determined indivisually for each device.

More attractive is the inherent continuous tuning behavior of the tunable twin-guide (TTG) DFB laser diode [1-22]. In this device a tuning layer with its own separate current path is transversely integrated with the active layer of a DFB laser. By carrier injection into this tuning layer, the refractive index of the DFB laser is changed homogeneously along the whole cavity length. This corresponds to a built-in simultaneous change of the Bragg wavelength and the optical phase, leading to a continuous tuning behavior with only one wavelength control current. The tuning range $\Delta\lambda_t$ of the continuously tunable laser diodes is limited by the maximum effective index change Δn_t as induced by the tuning to $\Delta\lambda_t/\lambda_0 <= |\Delta n_t|/n_e$, where λ_0 and ne denote the laser wavelength and the effective refractive index of the laser waveguide. With practical $|\Delta n_t|/n_e$-values

Regarding the coupling mechanism of the Bragg grating, the DFB and DBR lasers exploit the wavelength selection and feedback by the contradirectional coupling between the forward and backward propagating wave. Quite recently it has been shown, that essentially larger but discontinuous tuning ranges can be achieved using codirectionally coupling gratings. In this case, two codirectioanlly travelling modes of a twin-waveguide are resonantly coupled and the coupling wavelength is controlled by carrier injection into one of the waveguides.

Recently, Amann and coworkers proposed the distributed forward coupling (DFC) laser [1-23] that is able to provide wide range discontinuous tuning. It is based on the codirectional mode coupling along the laser cavity in a twin-guide structure. One of the main advantages is an unambiguous and simple wavelength tuning which is achieved by only one control current.

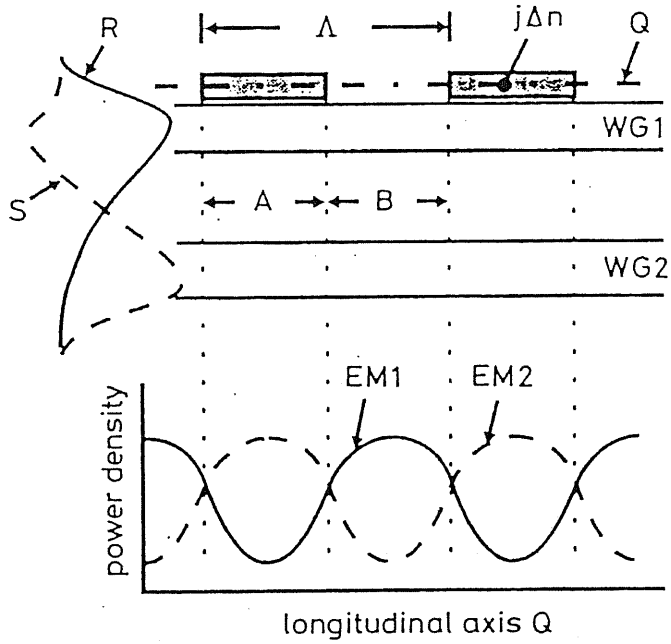

Figure 1-2 Schematic drawing of the longitudinal cross section of the distributed forward-coupling (DFC) laser.

1.2 Purpose and contents of this work

This doctor's thesis describes the results obtained from both a theoretical and an experimental study on widely tunable distributed forward- and backward-coupling (DFBC) lasers, comparing GC-DFBC with IC-DFBC lasers, and also describes the parameter-extraction technique (curve-fitting method) for semiconductor lasers.

We have proposed a new type of discontinuously-tunable laser, that is, distributed forward- and backward-coupling (DFBC) laser, and done a preliminary analysis by making use of the coupled-wave approach [1-24]. In the DFBC laser, the main mode is selected out of distributed feedback (DFB) modes rather than the Fabry-Perot modes in DFC lasers. Therefore, larger SMSR as well as the wide range tuning of the discontinuously-tunable lasers are expected.

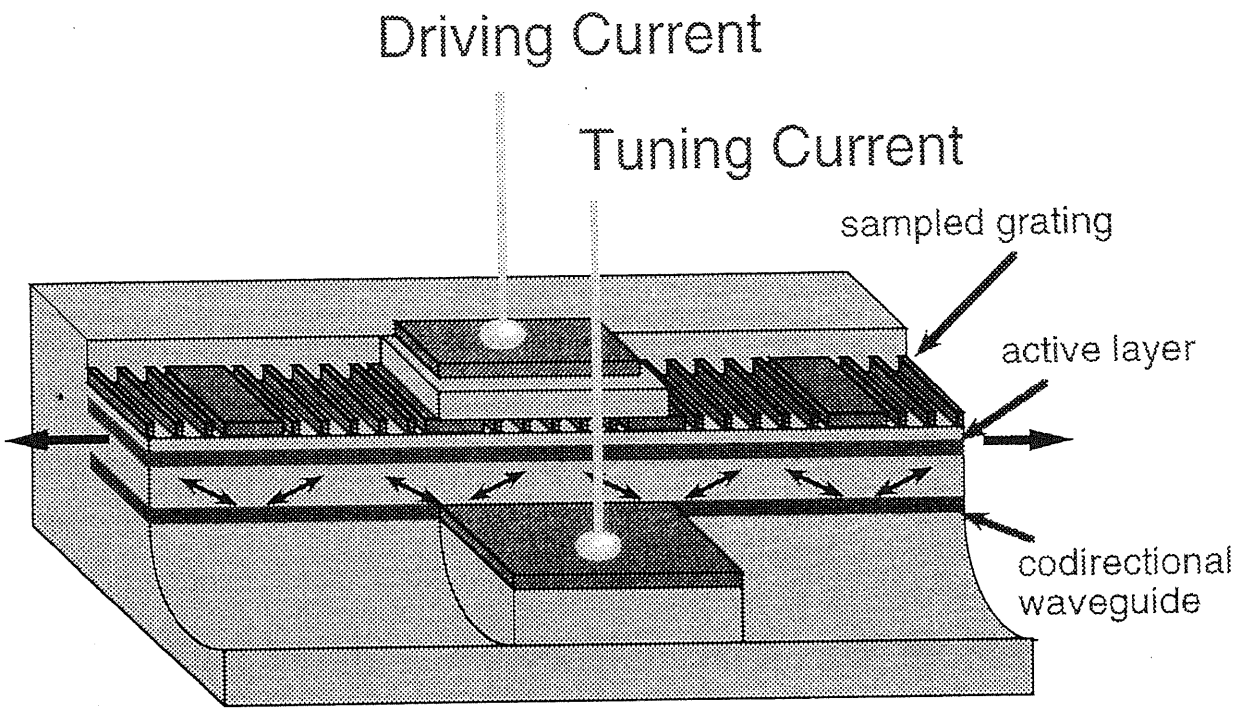

Figure 1-3 Schematic drawing of the longitudinal cross section of the distributed forward- and back ward-coupling (DFBC) laser.

This study is based on four pillars: First, introducing DFBC laser structure, explaining how it works. Second, the simulation results based on two theoretical approaches. Third, parameter extraction of semiconductor lasers, i.e., curve-fitting method, in order to extract not only index-coupling coefficient but also gain-coupling coefficient and other fundamental parameters, such as effective-refractive index, gain parameter of active layer, and linewidth enhancement factor. The last pillar is experimental work which describes details of the practical structure of DFBC lasers.

The second chapter gives a brief overview of the tuning mechanisms of DFBC laser. First, we describe the difference between continuously and discontinuously tunable lasers. Discontinuously tunable lasers normally show wider tuning range than continuously tnable lasers. Of cource, continuously tunable lasers

would be better for dense WDM which would be reallized in the near future. However for far future communication networks based on erbium-doped fiber amplifier (EDFA), discontinuously tunable lasers would be better because the bandwidth of erbium-doped fiber is more than 30 nm for 1.5 μm wavelength scheme. Then we introduce the structure of DFBC lasers which is a combination of sampled grating and codirectional coupler. The advantages of DFBC lasers are, simple operation (one-tuning-control-current), extremely wide tuning range, and possible for both index- and gain-coupling. Also we describe the tuning mechanisms of DFBC lasers.

In chapter 3, we show the simulation results of DFBC lasers. There are two approaches, one is to introduce 4X4 F-matrix derived from the four coupled-wave equations, and the other is to introduce mode-overlapping matrix at the border of the laser sections. Respectively, we explain the threshold condition of this model, and show the structures which are used in our simulations. We show the results of round-trip-gain calculations at a certain gain bias, and the lasing wavelength analysis at the threshold. We also show the internal field profile at one threshold condition. These calculations are done for purely gain-coupled DFBC lasers, and for purely index-coupled DFBC lasers.

In chapter 4, we describe parameter extraction of DFB lasers. Determination of the different device parameters of fabricated DFB laser diodes can be an important help in the further optimization of the laser design and even in systems design. First, we explain why it is so difficult to extract gain-coupling coefficient. Then we show our fitting procedure with a flow-chart. This fitting method is not totally automated, therefore at each process some parameters should be almost determined. Then we show measurements and fitting-results. We measured some spectra of GC-DFB laser diodes, and determined parameters.

In chapter 5, design of DFBC lasers is described. In order to simplify the

fabrication process of DFBC lasers, waveguides, layer structure, electrodes, photo-masks, and process of DFBC lasers are carefully designed. This particular structure requires only two epitaxial growth steps. The process for sampled gratings is also discussed.

In chapter 6, we show experimental results. Metal organic chemical vapor epitaxy (MOVPE) is used for the first epitaxial growth and the second growth. Before the second growth, sampled grating is formed by holographic exposure and lithography technique. After the second growth, we use seven photo-masks for the process.

In chapter 7, we conclude this paper. We have proposed a new type of widely tunable DFB lasers -- DFBC laser diodes -- which is a combination of sampled grating and codirectional forward coupler. This laser diode would provide more than 40 nm wavelength tuning range for 1.5 μm semiconductor lasers.

References in Chapter 1

[1-1] H. Kogelnik and C. V. Shank, "Coupled-wave theory of distributed feedback lasers", J. Appl. Phys., vol. 43, pp. 2327-2335, May 1972.

[1-2] Y. Luo, Y. Nakano, K. Tada, T. Inoue, H. Hosomatsu, and H. Iwaoka, "Gain-Coupled DFB Semiconductor Laser Having Corrugated Active Layer", Proc. of IOOC, Kobe, pp. 39-42, July 1989.

[1-3] S. R. Chin, "Effects of mirror reflectivity in a distributed-feedback laser", IEEE J. Quantum Electron., vol, QE-9, pp. 574-580, June 1973.

[1-4] W. Streifer, R. D. Burnham, and D. R. Scifres, "Effect of external reflectors on longitudinal modes of distributed feedback lasers", IEEE J. Quantum Electron., vol. QE-11, pp. 154-161, April 1975.

[1-5] Y. Luo, Y. Nakano, K. Tada, T. Inoue, H. Hosomatsu, and H. Iwaoka, "Purely gain-coupled distributed feedback semiconductor lasers", Appl. Phys. Lett., vol. 56, pp. 1620-1622, April 1990.

[1-6] Y. Nakano, Y. Luo, and K. Tada, "Facet reflection independent, single longitudinal mode oscillation in a GaAlAs/GaAs distributed feedback laser equipped with a gain-coupling mechanism", Appl. Phys. Lett. 55 (16), pp. 1606-1608, 1989.

[1-7] K. David, G. Morthier, P. Vankwikelberge, and R. Baets, "Yield analysis of non-AR-coated DFB lasers with combined index and gain coupling", Electron. Lett., 26, pp. 238-239, 1990.

[1-8] K. Kudo, J. I. Shim, K. Komori, and S. Arai, "Reduction of effective linewidth enhancement factor α_{eff} of DFB lasers with complex coupling coefficients", IEEE Photon. Technol. Lett., vol. 4, pp. 531-534, June 1992.

[1-9] A. J. Lowery, "Large-signal effective alpha factor of complex-coupled DFB semiconductor lasers", Electron. Lett., vol. 28, no. 25, pp. 2295-2297, Dec. 1992.

[1-10] B. Borchert, K. David, B. Stegmuller, R. Gessner, M. Beschorner, D. Sacher, and G. Franz, "1.55 μm gain-coupled uantum-well distributed feedback lasers with high single-mode yield and narrow linewidth", IEEE Photon. Technol. Lett., vol. 3, pp. 955-957, Nov. 1991.

[1-11] W. T. Tsang, F. S. Choa, M. C. Wu, Y. K. Chen, R. A. Logan, A. M. Sergent, and C. A. Burrus, "Long-wavelength InGaAsP/InP distributed feedback lasers

incorporating gain-coupled mechanism", IEEE Photon. Technol. Lett., vol 4, pp. 212-214, March 1992.

[1-12] G. P. Li, T. Makino, R. Moore, and N. Puetz, "1.55 μm Index/Gain coupled DFB lasers with strained layer multiquantum-well active grating", Electron. Lett., vol. 28, pp. 1726-1723, Aug. 1992.

[1-13] M. Suhara, S. Islam, and M. Yamada, "Criterion of external feedback sensitivity in index-coupled and gain-coupled DFB semiconductor lasers to be free from excess intensity noise", IEEE J. Quantum Electron., vol. 30, pp. 3-9, 1994.

[1-14] R. Hui, M. Kaveharad, and T. Makino, "External feedback sensitivity of partly gain-coupled DFB semiconductor lasers", IEEE Photon. Technol. Lett., vol. 6, pp. 897-899, 1994.

[1-15] H. Lu, G. P. Li, and T. Makino, "Spectral linewidth reduction in partly gain-coupled 1.55 μm strained multiple-quantum-well distributed feedback laser", Appl. Phys. Lett., vol. 29, no. 15, pp. 1367-1369, July 1993.

[1-16] Y. Luo, R. Takahashi, Y. Nakano, K. Tada, T. Kamiya, H. Hosomatsu, and H. Iwaoka, "Ultralow chirping short optical pulse (16ps) generation in gain-coupled distributed feedback semiconductor lasers", Appl. Phys. Lett., vol. 59, pp. 37-39, 1991.

[1-17] L. A. Coldren and S. W. Corzine, "Continuouly-tunable single-frequency semiconductor lasers", IEEE J. Quantum Electron., vol. 24, pp. 577-579, 1988.

[1-18] S. Murata, I. Mito, and K. Kobayashi, "Tuning ranges for 1.5 μm wavelength tunable DBR lasers", Electron. Lett., vol. 24, pp. 577-579, 1988.

[1-19] M.-C. Amann, "Linewidth enhancement in distributed-feedback semiconductor lasers", Electron. Lett., vol. 26, pp. 569-571, 1990..

[1-20] P. I. Kuindersma et al., "Tunable three-section, strained MQW, PA-DFB's with large single mode tuning range (72 A) and narrow linewidth (around 1 MHz)" in Conf. Dig. 12th IEEE Semiconductor Laser Conf. (Davos, Sqitzerland), 1990, pp. 248-249.

[1-21] S. Murata, I. Mito, and K. Kobayashi, "Over 720 GHz (5.8 nm) frequency tuning by a 1.5 mm DBR laser with phase and bragg wavelength control regions", Electron. Lettl, vol. 23, pp. 403-405, 1987.

[1-22] M.-C.Amann, S. Illek, C. Schanen, and W. Thulke, "Tuning range and threshold current of the tunable twin-guide (TTG) laser," IEEE Photon. Technol. Lett., vol. 1, pp. 253-254, 1989.

[1-23] M.-C. Amann, B. Borchert, S. Illek, and T. Wolf, "Widely tunable distributed forward coupled (DFC) laser," Electron. Lett., vol. 29, pp. 793-794, 1993.

[1-24] K. Sato, Y. Nakano, and K. Tada, "Wavelength tuning characteristics of widely tunable distributed forward- and backward-coupling semiconductor laser", IEEE Photon. Technol. Lett., pp. 257-259, Mar. 1995.

[1-25] P. Vankwikelberge, G. Morthier, and R. Baets, "CLADISS - A Longitudinal Multimode Model for the Analysis of the Static, Dynamic, and Stochastic Behavior of Diode Lasers with Distributed Feedback", IEEE J. Quantum Electron., vol. 26, pp. 1728-1741, Oct. 1990.

[1-26] G. Morthier, "Analysis of noise and spectral behaviour of DFB laser diodes", PhD thesis, University of Gent, 1991.

Chapter 2 DFBC lasers

2.1 Introductory remarks

Wavelength tunable lasers are required in the wavelength-division-multiplexed (WDM) photonic switching networks. Over the past several years, both continuously [2-1] and discontinuously [2-2][2-3][2-4][2-5] tunable lasers have been intensively studied. The latter ones are more feasible when over 20 nm tuning ranges are demanded.

Recently, Amann and coworkers proposed the distributed forward coupling (DFC) laser [2-6] that is able to provide wide range discontinuous tuning. It is based on the codirectional mode coupling along the laser cavity in a twin-guide structure. One of the main advantages is an unambiguous and simple wavelength tuning which is achieved by only one control current.

We have proposed another type of discontinuously-tunable laser, that is, distributed forward- and backward-coupling (DFBC) laser, and done a preliminary analysis by making use of the coupled-wave approach [2-7]. In the DFBC laser, the main mode is selected out of distributed feedback (DFB) modes rather than the Fabry-Perot modes in DFC lasers. Therefore, larger SMSR as well as the wide range tuning of the discontinuously-tunable lasers are expected.

Although the previous analysis was good for understanding tuning mechanism of the DFBC laser, the perturbative nature of the coupled-wave theory was not very appropriate when the twin waveguides were close to each other. In the next section, we investigate wavelength tuning characteristics of the DFBC laser by an eigen mode analysis, which is more rigorous and accurate than the previous

method.

2.2 Comparison of continuous and dis-continuous tuning

Here we describe the difference between continuous and discontinuous tuning. Continuous tuning is to tune the lasing wavelength continuously with changing the effective refractive index of the waveguide continuously. There is a relation between the wavelength and the effective refractive index as follows,

$$\frac{\Delta\lambda}{\lambda} \propto \frac{\Delta neff}{neff} \qquad (2\text{-}1),$$

where λ is the lasing wavelength, and n_{eff} is the effective refractive index of the waveguide. That is, the change of the wavelength is simply proportional to the change of the effective refractive index. However, the refractive index of the waveguide can only be changed at most 1 %, then the effective refractive index change is rather smaller than 1 %. For instance, the tuning range for the 1.55 μm wavelength scheme is as wide as 7 nm.

On the other hand, the tuning range of discontinuous tuning can be extremely wide when a combination of a semiconductor laser and a tunable wavelength filter is properly designed. The laser part provides many Fabry-Perot (FP) modes and the main mode is selected by the tunable wavelength filter. Here we discuss a combination of a DFB laser and a tunable filter. If the light is fed back by a sampled grating [2-2] or a super-structure-grating [2-4], the laser part provides many DFB reflection along the wavelength. Therefore the main mode of a discontinuously tunable laser is discretely selected by a tunable filter.

Here we focus on a wavelength filter based on forward-coupling. If there

exists two eigen modes in the waveguides, n_1 and n_2 are effective refractive indeces of the two eigen modes. The filter characteristics change when the difference of those two refractive indeces changes, then it results in a change of the wavelength of the main mode.

$$\frac{\Delta\lambda}{\lambda} \propto \frac{\Delta\delta n}{\delta n} \qquad (2\text{-}2)$$

Where $\delta n = n_1 - n_2$. Here δn is very small, therefore the change of the wavelength is extremely large. δn changes when the refractive index of one of the waveguides changes. For instance, the tuning range can be more than 70 nm (ten times wider than continuous tuning) for 1.55 μm wavelength scheme. However this tuning is discontinuous because the main mode is selected from the discrete FP-modes or DFB modes.

2.3 Structure of DFBC laser

Our DFBC laser is a sort of a combination of a DFB laser with sampled gratings and a widely tunable wavelength filter. Figure 2-1 shows a schematic drawing of a sampled grating and the round-trip-gain. There are many reflection peaks along the wavelength, and Figure 2-2 shows a schematic drawing of a grating-assisted codirectional coupler and the filter characteristics. As described in section 2.2 the filter characteristics are exteremly sensitive to the refractive index change in the waveguide.

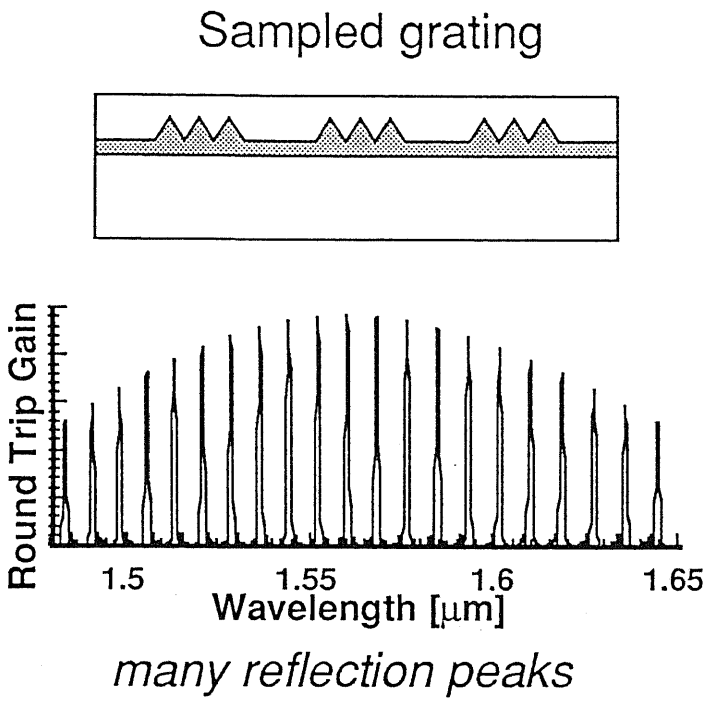

Figure 2-1 A schematic drawing of a sampled grating and the round-trip-gain.

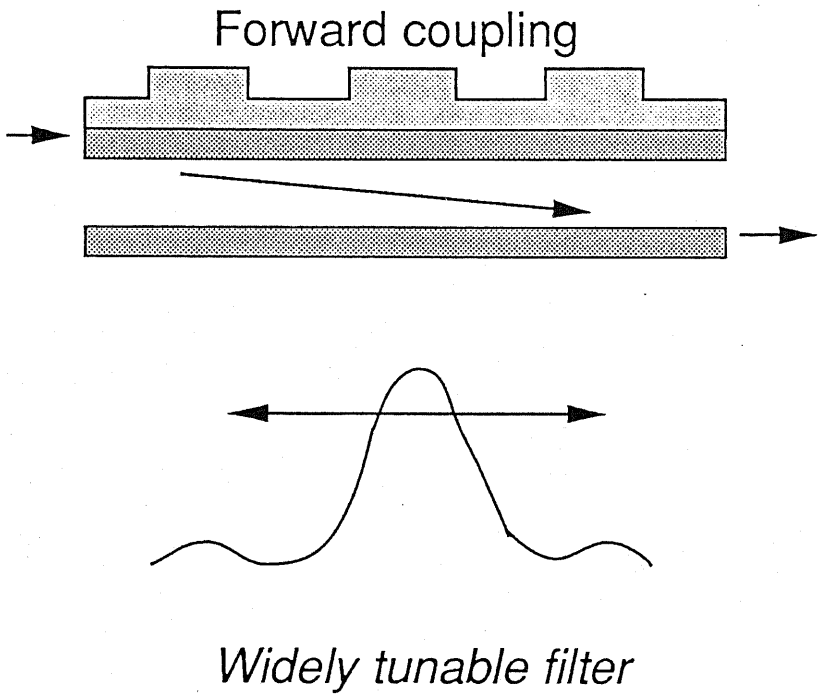

Figure 2-2 A schematic drawing of a grating-assisted codirectional coupler and the filter characteristics.

We propose a DFBC laser which is shown in Figure 2-3 which consists of a semiconductor laser and a codirectional coupler. The tuning mechanism is the same as a vertical-coupling-filter (VCF) [2-3] and a distributed forward-coupling (DFC) laser [2-6]. However in VCF and DFC laser, the main mode is selected from many Fabry-Perot oscillation modes, then the ambiguity of the main mode is a serious problem, i.e., the exact wavelength which is desired cannot be obtained. Moreover, the side-mode-suppression-retio (SMSR) of these lasers is not very large. In this study, we have solved this problem using a sampled grating which provides a Bragg feedback. Another advantage is that any type of grating is acceptable for this structure, for instance, gain-coupled grating. In addition, only one control current is needed to tune this laser. The simple operation is another advantage.

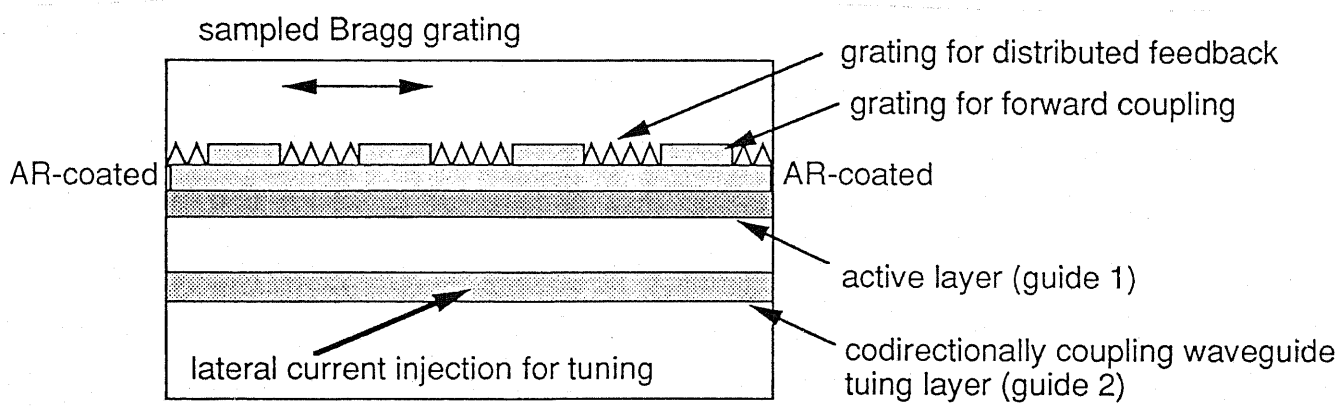

Figure 2-3 Schematic drawing of the longitudinal cross section of the distributed forward- and back ward-coupling (DFBC) laser.

2.4 Tuning mechanisms of DFBC laser

Figure 2-3 shows a schematic longitudinal cross section of the DFBC laser, which is basically a DFB laser diode incorporated with a sampled Bragg grating above the active layer and a codirectionally-coupled waveguide layer below the active layer. The whole waveguide is designed so as to hold the fundamental (even) and second-order (odd) transverse eigen modes.

When the light propagates across the border between the sections with and without the grating, the forward coupling occurs among the even and odd transverse modes in both sections. In the section with the grating, the odd transverse mode is designed to obtain much more gain and feedback from the grating than the even mode. Then, the odd transverse mode excite both even and odd modes in the section without grating and the light propagates zigzag between the two waveguides.

$$\Delta\beta Ln=2\pi N \qquad (2\text{-}3)$$

If the coupling period corresponding to a certain wavelength is equivalent to the sampling interval of the grating, the light is fed back most by the grating through the odd mode in the section with grating. This coupling period is very sensitive to change in the refractive index of the codirectional waveguide layer that can be induced by current injection into that layer. Small index change can give rise to a large change in the wavelength selected by the codirectional coupling and the sampled grating.

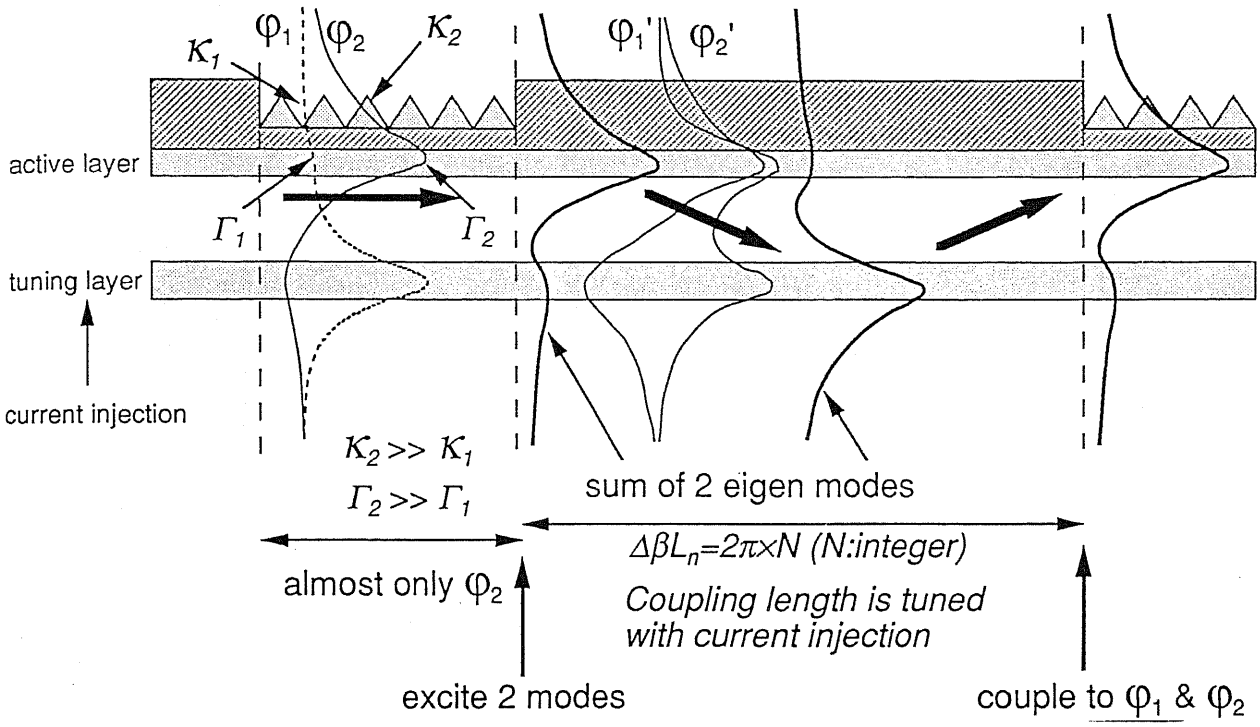

Figure 2-4 The tuning mechanism of DFBC lasers.

Actually, the above tunable filtering mechanism picks up one lasing mode out of a series of DFB modes produced by the grating sampling. The "channel" interval, i.e., the DFB mode spacing, is controllable through the sampling interval of the grating.

2.5 Summary

In summary, we have described a new tunable laser diode, i.e., the distributed forward- and backward-coupling (DFBC) laser. This laser is characterized by a codirectional forward coupling between two parallel waveguides together with a backward distributed Bragg feedback due to sampled grating. It would provide a wide tuning range (over 40 nm, for example) as well as larger SMSR in principle

compared with the other types of discontinuously-tunable laser diodes. Simple one current tuning scheme is another advantage of the DFBC laser. Either gain or index coupling, or a combination of these may be used with the DFBC laser. However, the gain coupling is preferable as it could lead to larger SMSR. For fabrication this kind of laser has a big advantage because the active layer and the codirectional waveguide are placed on different level of layers. If the active layer and the codirectional waveguide are placed on the same leve [2-5], the cristal growth can not be performed at one time.

References in Chapter 2

[2-1] M.-C.Amann, S. Illek, C. Schanen, and W. Thulke, "Tuning range and threshold current of the tunable twin-guide (TTG) laser," IEEE Photon. Technol. Lett., vol. 1, pp. 253-254, 1989.

[2-2] V. Jayaraman, A. Mathur, L. A. Coldren, and P. D. Dapkus, "Extended tuning range in sampled grating DBR lasers," IEEE Photon. Technol. Lett., vol. 5, pp. 489-491, 1993.

[2-3] R. C. Alferness, T. L. Koch, L. L. Buhl, F. Storz, F. Heismann, and M. J. R. Martyak, "Grating-assisted InGaAsP/InP vertical codirectional coupler filter," Appl. Phys. Lett., vol. 55, pp. 2011-2013, 1989.

[2-4] Y. Tohmori, F. Kano, H. Ishii, Y. Yoshikuni, and Y. Kondo, "Wide tuning with narrow linewidth in DFB lasers with superstructure grating (SSG)," Electron. Lett., vol. 29, pp. 1350-1352, 1993.

[2-5] J. Willems, G. Morthier, R. Baets, "Novel widely tunable integrated optical filter

with high spectral selectivity", European Conference on Optical Communication (ECOC'92), pp. 413-416, 1992.

[2-6] M.-C. Amann, B. Borchert, S. Illek, and T. Wolf, "Widely tunable distributed forward coupled (DFC) laser," Electron. Lett., vol. 29, pp. 793-794, 1993.

[2-7] K. Sato, Y. Nakano, and K. Tada, "Wavelength Tuning Characteristics of Widely Tunable Distributed Forward- and Backward-Coupling Semiconductor Laser", IEEE Photon. Technol. Lett., pp. 257-259, Mar. 1995.

[2-8] H.-P. Nolting and G. Sztefka, "Eigenmode Matching and Propagation Theory of Square Meander-Type Couplers", IEEE Photon. Technol. Lett., vol. 4, pp. 1386-1389, Dec. 1992.

[2-9] Vankwikelberge, G. Morthier, and R. Baets, "CLADISS - A Longitudinal Multimode Model for the Analysis of the Static, Dynamic, and Stochastic Behavior of Diode Lasers with Distributed Feedback", IEEE J. Quantum Electron., vol. 26, pp. 1728-1741, Oct. 1990.

[2-10] Y. Luo, Y. Nakano, K. Tada, T. Inoue, H. Hosomatsu, and H. Iwaoka , "Purely gain-coupled distributed feedback semiconductor lasers," Appl. Phys Lett., vol. 56, pp. 1620-1622, 1990.

Chapter 3 Simulation of DFBC lasers

3.1 Introductory remarks

In this chapter the distributed forward- and backward-coupling (DFBC) semiconductor laser for wide wavelength tuning is proposed and analyzed. A four-dimensional F-matrix method is established in order to pursue the numerical simulation. As a result, over 100 nm tuning around 1.55 μm by simple injection current control scheme is predicted.

We have developed the new theories to handle the particular structure such as a laser diode which consists of Bragg and forward-coupling gratings. Here we show these two methods as follows,

1. Coupled-mode analysis
2. Mode-expansion analysis

Coupled-mode analysis here is an extended version of general 2X2 F-matrix method. We have derived 4X4 F-matrix including forward-coupling as well as backward-coupling from Brag gratings. In this analysis, the complex amplitudes of forward- and backward-going wave are assumed to be gradually varying functions along the laser cavity. The point of this analysis is that we have omitted the Bragg feedback of one of the eigen modes because the selectivity of the wavelength is generated when only the other eigen mode is fed back by the Bragg gratings.

Then we have applied mode-expansion method for the analysis of DFBC lasers. In this analysis, we use general F-matrix in both Bragg-grating and non Bragg-grating section along the cavity, and the overlap-matrix at the borders

between Bragg-grating and non Bragg-grating section. We investigate wavelength tuning characteristics of the DFBC laser by an eigen mode analysis, which is more rigorous and accurate than the previous method. At the borders, the intensity of the light is continuous, however the magnitude of each eigen mode is not continuous. The point is that the Bragg feedback of the two eigen modes is taken into account in this analysis.

If the duty of the sampled grating is small, above two methods would be closer. The first coupled-mode approach is rather good in order to understand the tuning mechanisms of DFBC lasers, and it gives a good approximation. However the perturbative nature of the coupled-wave theory was not very appropriate when the twin waveguides were close to each other. In this chapter we show the wavelength tuning characteristics of DFBC lasers by both two methods. The first coupled-mode analysis is still useful because we assumed the duty cycle of the sampled grating to be rather small (10 %).

3.2 Coupled-mode analysis

3.2.1 Introducing 4X4 F-matrices

We introduce envelope complex amplitudes, R, as functions of z-coordinate along the laser cavity, which are related to the complex electrical field amplitudes, E, as

$$E_T^{\pm}(z) = R_T^{\pm}(z)\, e^{\mp j\beta_2 z} \qquad (3\text{-}1)\ (a)$$

$$E_1^{\pm}(z) = R_1^{\pm}(z)\, e^{\mp j\beta_2 z} \qquad (3\text{-}1)\ (b)$$

Here, the superscripts + and - indicate forward and backward waves, and the subscripts 1 and 2 denote the upper waveguide (the active layer, guide 1) and the lower codirectional waveguide (guide 2). β_2 is the propagation constant of the guide 2.

In order to handle distributed feedback and codirectional coupling systems at the same time, we present the following four coupled wave equations:

$$\frac{\partial R_1^+}{\partial z} + j(\beta_1 - \beta_2) R_1^+ = \kappa_{FB} R_1^- e^{2j(\beta_2 - \beta_g)z} + \kappa_{12}^* R_2^- \qquad (3\text{-}2)\ (a)$$

$$-\frac{\partial R_1^-}{\partial z} + j(\beta_1 - \beta_2) R_1^- = \kappa_{BF} R_1^+ e^{-2j(\beta_2 - \beta_g)z} + \kappa_{12}^* R_2^- \qquad (3\text{-}2)\ (b)$$

$$\frac{\partial R_2^+}{\partial z} = \kappa_{21} R_1^+ \qquad (3\text{-}2)\ (c)$$

$$-\frac{\partial R_2^+}{\partial z} = \kappa_{21}^* R_1^- \qquad (3\text{-}2)\ (d)$$

Here, β_g is π/Λ, Λ the grating pitch, κ_{FB}, κ_{BF} the coupling coefficients of the distributed feedback, and κ_{12}, κ_{21} the coupling coefficients of the codirectional coupling between guides 1 and 2. β_1 is the propagation constant of the active layer (guide 1). There are two reasons for us to have neglected the backward scattering of R_2 in the equations (3-2) (c) and (3-2) (d). One of them is that, as mentioned above, the energy transfer is as large as 84 % or more. This means that R_2 becomes very small where the diffraction grating appears. The other reason is the difference in the transverse field profile. The waveguide 2 is at farther distance from

the grating than the waveguide 1, and therefore the optical confinement factor into the grating layer of the transverse mode associated with R_2 is smaller. In addition, the confinement factor into the waveguide 2 is made larger than that into the guide 1. In other words, the transverse layer structure should be designed in such a way that the R_1-related transverse mode penetrates into the grating much but the R_2 mode doesn't.

From the equations (3-2), we obtained these equations,

$$\frac{\partial^2 R_1^+}{\partial z} + j\Delta\beta \frac{\partial R_1^+}{\partial z} - \kappa_{FB} \frac{\partial}{\partial z}(R_1^- e^{2j\Delta\beta_2 z}) = \kappa_{12}\kappa_{21} R_1^+ \qquad (3\text{-}3)\ (a)$$

$$\frac{\partial^2 R_1^-}{\partial z^2} - j\Delta\beta \frac{\partial R_1^-}{\partial z} + \kappa_{BF} \frac{\partial}{\partial z}(R_1^+ e^{-2j\Delta\beta_2 z}) = \kappa_{12}^* \kappa_{21}^* R_2^- \qquad (3\text{-}3)\ (b),$$

where $\Delta\beta = \beta_1 - \beta_2$, $\Delta\beta_2 = \beta_2 - \beta_g$, and $\beta_g = \pi/\Lambda$. Equation (3-3) (a) gives a solution for R_1^-, as follows,

$$R_1^- = \frac{e^{-2j\Delta\beta_2 z}}{\kappa_{FB}} \left(\frac{\partial R_1^+}{\partial z} + j\Delta\beta R_1^+ - \kappa_{12}\kappa_{21} \int R_1^+ \right) \qquad (3\text{-}3)\ (c)$$

Equation (3-3) (b) also gives,

$$\frac{\partial}{\partial z}\left(\frac{\partial R_1^-}{\partial z} - j\Delta\beta R_1^- - \kappa_{BF} R_1^+ e^{-2j\Delta\beta_2 z} \right) = \kappa_{12}^* \kappa_{21}^* R_1^- \qquad (3\text{-}3)\ (d)$$

With equation (3-3) (c), the following fourth-order differential equation is derived

from equation (3-3) (d),

$$\frac{\partial^4 R_1^+}{\partial z^4}+a\frac{\partial^3 R_1^+}{\partial z^3}+b\frac{\partial^2 R_1^+}{\partial z^2}+c\frac{\partial R_1^+}{\partial z}+d=0 \qquad (3\text{-}4),$$

where

$$a=-4j\Delta\beta_2 \qquad (3\text{-}5)\ (a)$$

$$b=\Delta\beta^2+\kappa_{FB}\kappa_{BF}-\kappa_{12}\kappa_{21}-\kappa_{12}^*\kappa_{21}^*+2\Delta\beta_2(\Delta\beta-2\Delta\beta_2) \qquad (3\text{-}5)\ (b)$$

$$c=j\kappa_{12}\kappa_{21}(4\Delta\beta_2+\Delta\beta)-j\Delta\beta\kappa_{12}^*\kappa_{21}^*-2j\Delta\beta_2\kappa_{FB}\kappa_{BF}-2j\Delta\beta_2\Delta\beta(\Delta\beta+2\Delta\beta_2) \qquad (3\text{-}5)\ (c)$$

$$d=\kappa_{12}\kappa_{21}(2\Delta\beta_2(2\Delta\beta_2+\Delta\beta)+\kappa_{12}^*\kappa_{21}^*) \qquad (3\text{-}5)\ (d)$$

Then we obtain the solutions of R, as follows,

$$R_1^+=C_1e^{\gamma_1 z}+C_2e^{\gamma_2 z}+C_3e^{\gamma_3 z}+C_4e^{\gamma_3 z} \qquad (3\text{-}6)\ (a)$$

$$R_1^-=\frac{1}{\kappa_{FB}}\{(j\Delta\beta+\gamma_1-\frac{\kappa_{12}\kappa_{21}}{\gamma_1})C_1e^{(\gamma_1-2j\Delta\beta_2)z}+(j\Delta\beta+\gamma_2-\frac{\kappa_{12}\kappa_{21}}{\gamma_2})C_2e^{(\gamma_2-2j\Delta\beta_2)z}$$
$$+(j\Delta\beta+\gamma_3-\frac{\kappa_{12}\kappa_{21}}{\gamma_3})C_3e^{(\gamma_3-2j\Delta\beta_2)z}+(j\Delta\beta+\gamma_4-\frac{\kappa_{12}\kappa_{21}}{\gamma_4})C_4e^{(\gamma_4-2j\Delta\beta_2)z}\} \qquad (3\text{-}6)\ (b)$$

$$R_2^+=\frac{K_{21}}{\gamma_1}C_1e^{\gamma_1 z}+\frac{K_{21}}{\gamma_2}C_2e^{\gamma_2 z}+\frac{K_{21}}{\gamma_3}C_3e^{\gamma_3 z}+\frac{K_{21}}{\gamma_4}C_4e^{\gamma_3 z} \qquad (3\text{-}6)\ (c)$$

$$R_1^-=\frac{1}{K_{12}^*K_{FB}}\{(j\Delta\beta-\gamma_1+2j\Delta\beta_2)(j\Delta\beta+\gamma_1-\frac{K_{12}K_{21}}{\gamma_1})-K_{FB}K_{BF})C_1e^{(\gamma_1-2j\Delta\beta_2)z}+(j\Delta\beta-\gamma_2+2j\Delta\beta_2)(j\Delta\beta+\gamma_2-\frac{K_{12}K_{21}}{\gamma_2})-K_{FB}K_{BF})C_2e^{(\gamma_2-2j\Delta\beta_2)z}$$
$$+(j\Delta\beta-\gamma_3+2j\Delta\beta_2)(j\Delta\beta+\gamma_3-\frac{K_{12}K_{21}}{\gamma_3})-K_{FB}K_{BF})C_3e^{(\gamma_3-2j\Delta\beta_2)z}+(j\Delta\beta-\gamma_4+2j\Delta\beta_2)(j\Delta\beta+\gamma_4-\frac{K_{12}K_{21}}{\gamma_4})-K_{FB}K_{BF})C_4e^{(\gamma_4-2j\Delta\beta_2)z}\}$$

(3-6) (d),

where γ_i are the characteristic roots of the fourth-order differential equation derived from equation (3-4), C_i's are undefined constants derived from the differential equation (3-4). Here we define C and T matrices and the i-th columns of the matrices C and T are as follows,

$$C_i=\begin{pmatrix}1\\ u_i\\ K_{21}/\gamma_i\\ u_iv_i-K_{BF}/K_{12}^*\end{pmatrix} \qquad (3\text{-}7)$$

$$T_i=\begin{pmatrix}1\\ u_ie^{-2j(\beta_2-\beta_g)z_1}\\ K_{21}/\gamma_i\\ (u_iv_i-K_{BF}/K_{12}^*)e^{-2j(\beta_2-\beta_g)z_1}\end{pmatrix}e^{\gamma_i z_1} \qquad (3\text{-}8),$$

where C^{-1} is the inverse matrix of C, and $u_i=\{j(\beta_1-\beta_2)+\gamma_i-K_{12}K_{21}/\gamma_i\}/K_{FB}$, $v_i=\{j(\beta_1+\beta_2-2\beta_g)-\gamma_i\}/K_{12}^*$.

A four-dimensional F-matrix from z=0 to $z=z_1$, F, is derived from these equations as

$$F=PTC^{-1} \qquad (3\text{-}9)$$

$$\begin{pmatrix} E_1^+(z_1) \\ E_1^-(z_1) \\ E_2^+(z_1) \\ E_2^-(z_1) \end{pmatrix} = F \begin{pmatrix} E_1^+(0) \\ E_1^-(0) \\ E_2^+(0) \\ E_2^-(0) \end{pmatrix} \tag{3-10}$$

where P is the transformation which converts vector R_j into E_j, as follows

$$P = \begin{pmatrix} e^{-j\beta_2 z} & 0 & 0 & 0 \\ 0 & e^{j\beta_2 z} & 0 & 0 \\ 0 & 0 & e^{-j\beta_2 z} & 0 \\ 0 & 0 & 0 & e^{j\beta_2 z} \end{pmatrix} \tag{3-11}$$

Like the ordinary lasers [3-6], the resonance condition is satisfied when the absolute value of the complex round trip gain becomes 1 and its phase becomes 0:

$$|\rho_L \cdot \rho_R| = 1 \tag{3-12}$$

Here, ρ_L and ρ_R are the effective reflectivities corresponding to the left and right halves of the cavity.

If the both end facets are anti-reflection (AR) coated, these effective reflectivities are expressed as

$$\rho_L = \frac{F_{24}F_{L12} - F_{22}F_{L14}}{F_{24}F_{L22} - F_{22}F_{L24}} \tag{3-13 (a)}$$

$$\rho_R = \frac{F_{13}^{-1}F_{L12}^{-1} - F_{11}^{-1}F_{R23}^{-1}}{F_{13}^{-1}F_{R11}^{-1} - F_{11}^{-1}F_{R13}^{-1}} \tag{3-13 (b)}$$

where F_{ij} is the ij-th element of the matrix F which is the product of the local F-matrix from z=0 to z=L (L is cavity length). F^{-1} is the inverse matrix of F. F_{Lij} is the ij-th element of the matrix F_L which is the product of the local F-matrix from z=0 to z=L/2, and F_{Rij}^{-1} is the element of the inverse matrix of F_R, the product of the local F-matrix from z=L/2 to z=L.

3.2.2 Simulation results

Simulation has been carried out around 1.55 μm wavelength. Figure 3-1 shows the assumed refractive indices (taken from Reference [3-7]) of each layer. The active and the grating layers are assumed to be one upper waveguide with an effective index n_{active}. We also assumed that the upper and the lower waveguides are of 0.125 μm and 0.2 μm thickness, respectively. n_{active} is fixed at 3.495. On the other hand, the refractive index of the codirectional waveguide (n_{guide}) was taken as a variable parameter, and was varied from 3.325 to 3.355. This sort of index change is available by injecting carriers into the lower waveguide region.

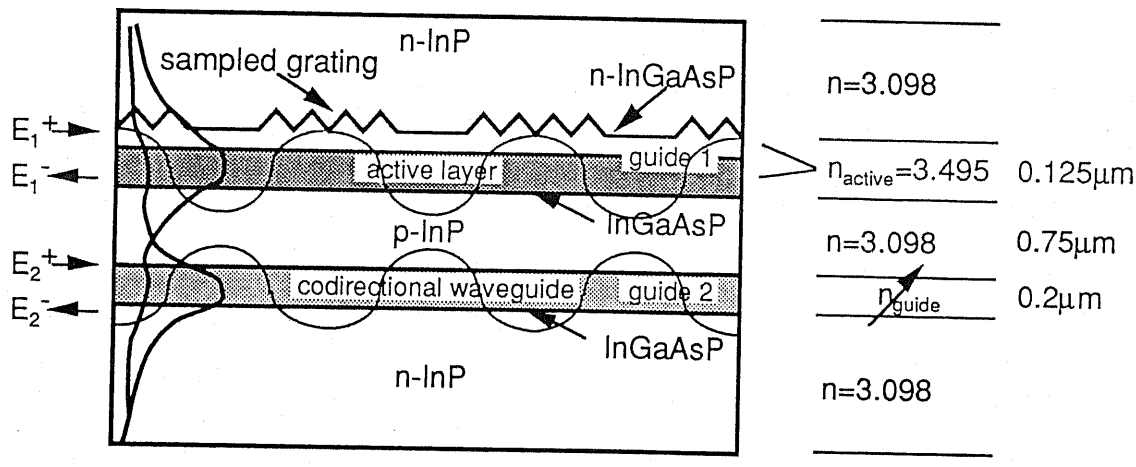

Figure 3-1 Schematic drawing of the longitudinal cross section of the distributed forward- and backward-coupling (DFBC)laser.

Refractive indices of the cladding and the spacing layers are assumed to be identical, i.e., 3.098. Thickness of the spacing layer is 0.75 μm. The distributed feedback here is assumed to be of pure gain coupling [3-8] with a coupling coefficient of 50 cm^{-1}. The coefficient of the codirectional coupling is dependent on the wavelength and n_{guide}. In other words, when the nguide is changed, the electrical field profile and the effective refractive index are changed, then the coupling strength between the two waveguides is changed. The material dispersion is also taken into account. In this particular example we have changed n_{guide} from 3.325 to 3.355, then we have obtained the codirectional coupling from 0.062 μm^{-1} to 0.060 μm^{-1} for the wavelength 1.55 μm. The sampling interval of the grating is 50 μm, and its duty cycle is 4 % in order to obtain sampled DFB modes with small gain difference over a wide wavelength range. We assumed AR-coated devices with the cavity length of 600 μm.

Figure 3-2 (a), (b), and (c) show calculated amplitudes of the round trip gain versus wavelength at three different refractive index values in the codirectional waveguide. The spikes in these figures correspond to sampled DFB modes. The gradual wavelength dependence (or the envelope) is mainly incorporated by the codirectional forward coupling effect. Since the envelope moves very fast with the index change, the mode with the largest gain (lasing mode) could be selected from a wide range of wavelength. Moreover, since each mode is established by the distributed feedback, mode competition among longitudinal (Fabry-Perot-like) modes is minimal. Therefore, large SMSR is expected in general. From this point of view, use of gain coupling rather than index coupling is advantageous.

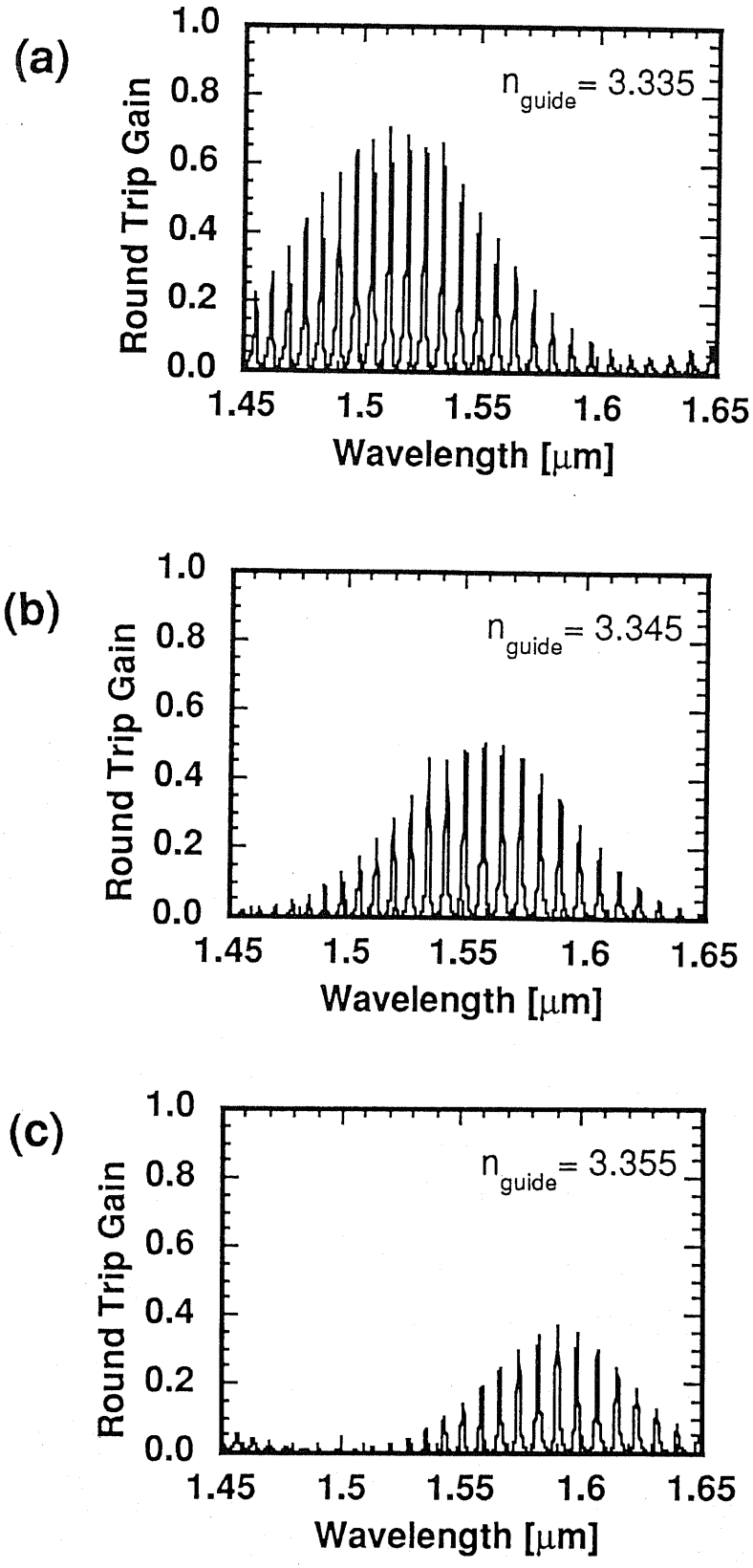

Figure 3-2 Wavelength dependence of the round-trip-gain in the DFBC laser with the refractive index of the codirectional waveguide layer being 3.335 (a), 3.345 (b), and 3.355 (c).

Figure 3-3 shows simulated tuning characteristics of lasing wavelength at threshold. Although the refractive index change in the codirectional waveguide is as small as 0.03, a tuning range as large as 100 nm is obtained in the figure. It is possible to design other structures having narrower mode gaps or different tuning ranges by changing the device parameters such as the cavity length, the sampling duty cycle of the grating, the coupling length of the codirectional waveguides, etc.

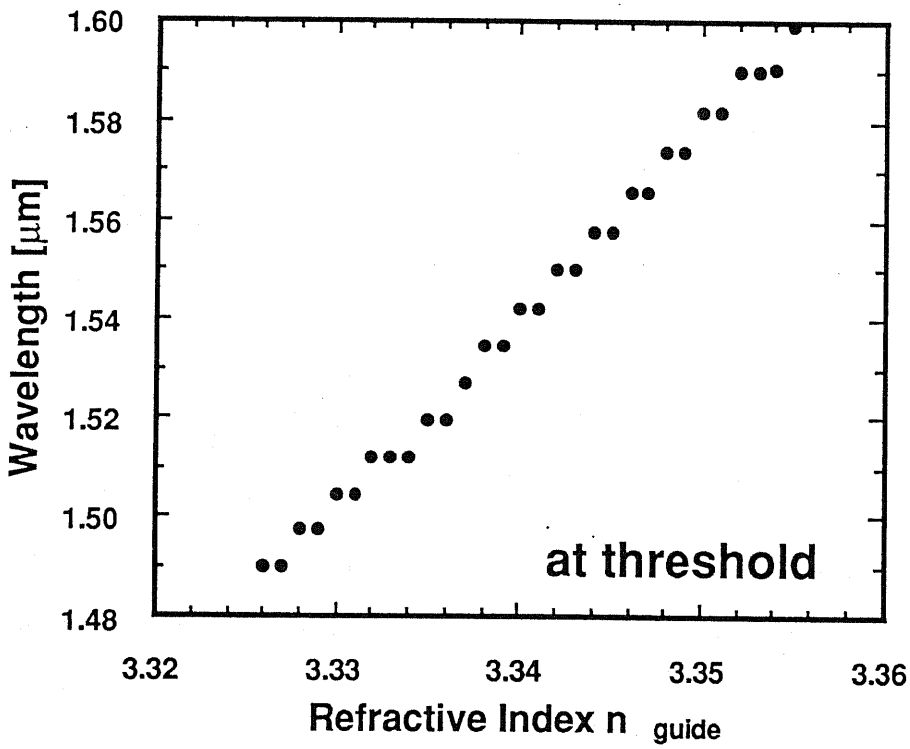

Figure 3-3 An example of simulated wavelength tuning characteristics of the DFBC laser exhibiting a tuning range over 100 nm around 1.55 μm.

We have shown simulation results of only gain-coupled (GC) DFBC lasers in Figure 3-3. In order to compare GC-DFBC lasers with IC-DFBC lasers, we show wavelength tuning characteristics of both GC- and IC-DFBC lasers in Figure 3-4. The coupling coefficients are both 50 cm^{-1}. The other parameters are the same as used in Figure 3-3. In Figure 3-4, IC-DFBC laser shows wider tuning range than

GC-DFBC laser. It means that GC-DFB lasers have more stable main mode. Of course the main mode of tunable lasers is desired to be stable when the wavelength is selected. In that sence, tunable GC-DFB lasers are more advantageous than IC-DFB lasers.

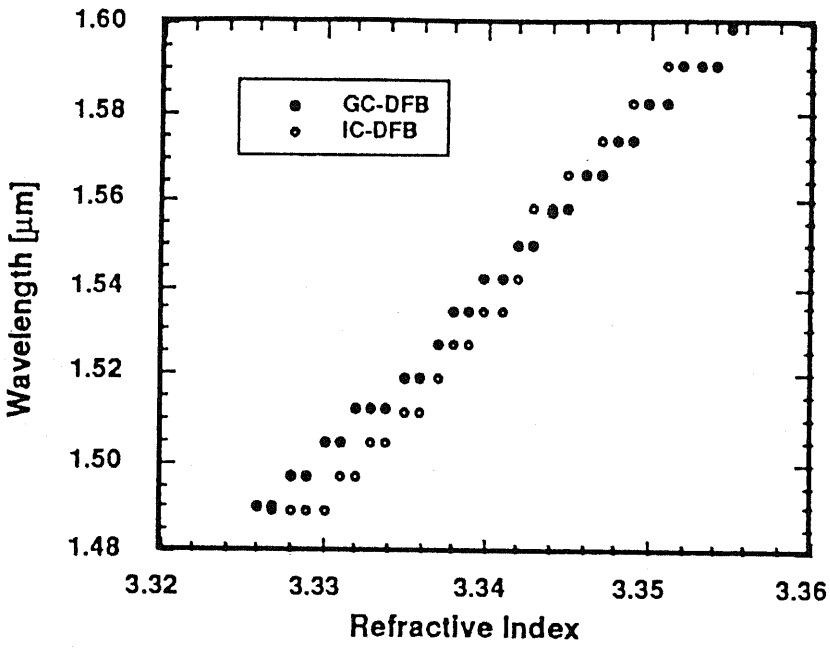

Figure 3-4 An example of simulated wavelength tuning characteristics of the DFBC laser exhibiting a tuning range over 100 nm around 1.55 μm. GC-DFB (black dots) and IC-DFB (white dots).

3.2.3 Discussions

As a conclusion, we have presented a new tunable laser diode, the distributed forward- and backward-coupling (DFBC) laser, which is characterized by a codirectional forward coupling between two parallel waveguides together with a backward distributed Bragg feedback due to a sampled grating. It would provide a wide tuning range (over 100 nm, for example) as well as larger SMSR in principle

compared with the other types of discontinuously-tunable laser diodes. Simple one current tuning scheme is another advantage of the DFBC laser. Either gain or index coupling, or a combination of these may be used with the DFBC laser. However, the gain coupling is preferable as it could lead to larger SMSR.

3.3 Mode-expansion analysis

3.3.4 Introducing expansion coefficients

We introduce envelope complex amplitudes, R's, as functions of z-coordinate along the laser cavity, which are related to the complex electrical field amplitudes, E's, as

$$E^{\pm}(x,y,z)=R_1^{\pm}(z)\varphi_1(x,y)e^{\mp j\beta_1 z}+R_2^{\pm}(z)\varphi_2(x,y)e^{\mp j\beta_2 z} \qquad (3\text{-}14)$$

Here, the superscripts + and - indicate forward and backward waves, φ_1 and φ_2 are the transverse eigen modes of the waveguide, and the subscripts 1 and 2 denotes the even and odd modes, respectively. β_1 and β_2 are the propagation constants of the mode 1 and mode 2.

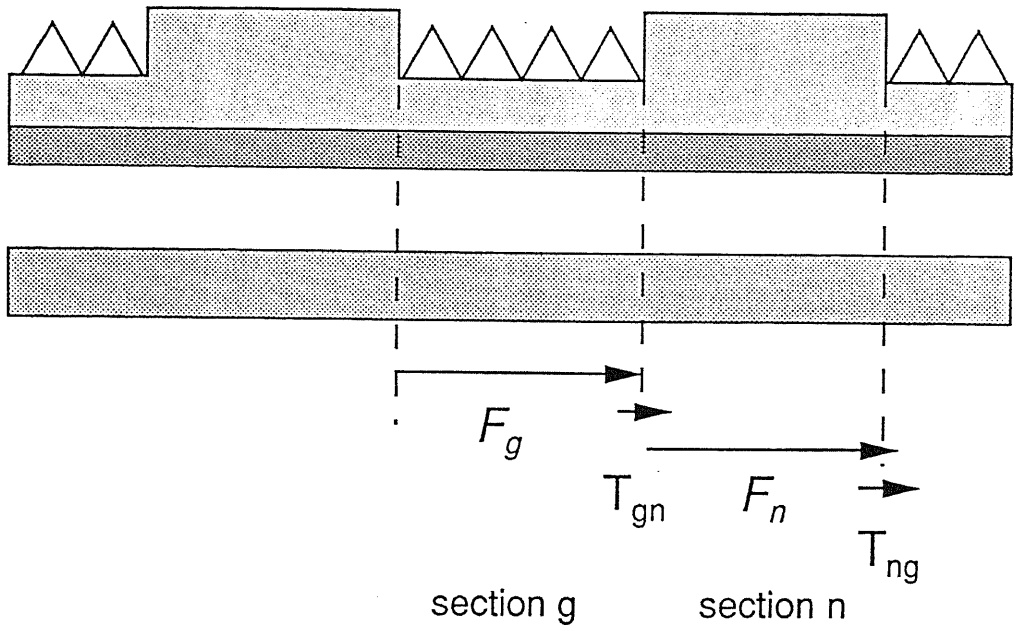

Figure 3-5 Schematic drawing of the longitudinal cross section of the distributed forward- and backward-coupling (DFBC) laser.

A 4 X 4 F-matrix, F, for the grating and the non-grating section pair from $z=z_k$ to $z=z_{k+1}$ in Figure 3-5 relates R's at both ends by equation (3-15), and F itself is expressed by equation (3-16):

$$\begin{pmatrix} R_1^+(z_{k+1}) \\ R_1^-(z_{k+1}) \\ R_2^+(z_{k+1}) \\ R_2^-(z_{k+1}) \end{pmatrix} = F \begin{pmatrix} R_1^+(z_k) \\ R_1^-(z_k) \\ R_2^+(z_k) \\ R_2^-(z_k) \end{pmatrix} \qquad (3\text{-}15)$$

$$F = T_{ng} F_n T_{gn} F_g \qquad (3\text{-}16)$$

Symbols "g" and "n" denote the sections with and without grating, respectively. T_{gn} and T_{ng} are the transfer matrices at the section border, and F_g and F_n are the

F-matrices for each section, shown in Figure 3-5. They are explicitly written as

$$T_{gn}=\begin{pmatrix} a_{11} & 0 & a_{21} & 0 \\ 0 & a_{11} & 0 & a_{12} \\ a_{12} & 0 & a_{22} & 0 \\ 0 & a_{21} & 0 & a_{22} \end{pmatrix} \tag{3-17}$$

$$F_g=\begin{pmatrix} F_{1g} & 0 \\ 0 & F_{2g} \end{pmatrix} \tag{3-18}$$

where a_{ij} is the expansion coefficient from reference [3-11]. Here, the reflection at the borders of the sections is not taken into account. a_{ij} is expressed like this,

$$a_{ij}=\int_{-\infty}^{\infty} \varphi_i \varphi_j' dx \tag{3-19}$$

where,

$$R_{1g}^{+}\varphi_1+R_{2g}^{+}\varphi_2=R_{1n}^{+}\varphi_1'+R_{2n}^{+}\varphi_2' \tag{3-20}$$

F_{1g} and F_{2g} are the DFB 2 X 2 F-matrices [3-6] of the modes 1 and 2. T_{ng} and F_n can be expressed in similar forms.

$$F=\begin{pmatrix} \cosh\gamma z-\frac{j\Delta\beta}{\gamma}\sinh\gamma z & -\frac{\kappa_{FB}}{\gamma}\sinh\gamma z \\ -\frac{\kappa_{BF}}{\gamma}\sinh\gamma z & \cosh\gamma z+\frac{j\Delta\beta}{\gamma}\sinh\gamma z \end{pmatrix} \tag{3-21}$$

where γ is satisfied with

$$\gamma=\sqrt{-\Delta\beta^2-\kappa_{FB}\kappa_{BF}} \qquad (3\text{-}22)$$

and $\Delta\beta = \beta - \beta_g$.

Figure 3-6 The round-trip-gain of the DFBC laser.

The round trip gain can be calculated by making use of the above F-matrix for the grating-nongrating pair. In Figure 3-6 we defined the reflection matrix of two eigen modes,

$$\begin{pmatrix} R_1^+ \\ R_2^+ \end{pmatrix}=\begin{pmatrix} \rho_{L11} & \rho_{L21} \\ \rho_{L12} & \rho_{L22} \end{pmatrix}\begin{pmatrix} R_1^- \\ R_2^- \end{pmatrix} \qquad (3\text{-}23)\ (a)$$

$$\begin{pmatrix} R_1^- \\ R_2^- \end{pmatrix}=\begin{pmatrix} \rho_{R11} & \rho_{R21} \\ \rho_{R12} & \rho_{R22} \end{pmatrix}\begin{pmatrix} R_1^+ \\ R_2^+ \end{pmatrix} \qquad (3\text{-}23)\ (b)$$

Here the cavity of the DFBC laser is devided into two parts. The matrix F_L is the product of the local F-matrix from z=0 to z=L/2, and the matrix F_R is the product of the local F-matrix from z=L/2 to z=L. ρ_L and ρ_R are the elements of the matrix F_L and F_R, respectively. Therefore we define the round-trip-gain matrix as follows,

$$\rho\equiv\begin{pmatrix} \rho_{11} & \rho_{21} \\ \rho_{12} & \rho_{22} \end{pmatrix}=\begin{pmatrix} \rho_{L11} & \rho_{L21} \\ \rho_{L12} & \rho_{L22} \end{pmatrix}\begin{pmatrix} \rho_{R11} & \rho_{R21} \\ \rho_{R12} & \rho_{R22} \end{pmatrix} \qquad (3\text{-}24)$$

Therefore the resonance condition of the DFBC laser is expressed with a unit matrix E,

$$E=\begin{pmatrix} 1 & 0 \\ 0 & 1 \end{pmatrix} \tag{3-25}$$

$$E\begin{pmatrix} R_1^+ \\ R_2^+ \end{pmatrix}=\rho\begin{pmatrix} R_1^+ \\ R_2^+ \end{pmatrix} \tag{3-26}$$

That is,

$$\rho_{11}+\rho_{22}+\rho_{12}\rho_{21}-\rho_{11}\rho_{22}=1 \tag{3-27}$$

Here we define the equation (3-27) to be a round-trip-gain of DFBC laser. Like the ordinary lasers [3-6], the resonance condition is satisfied when the absolute value of the complex round trip gain becomes 1 and its phase becomes 0.

3.3.5 Simulation results

Simulation has been carried out around 1.55 μm wavelength. Assumed thickness of each layer is shown in Figure 3-7. The refractive index of the active layer (n_{active}), the substrate, and the grating layer of the forward coupling are fixed at 3.41 , 3.1, and 3.215, respectively, whereas the refractive index of the codirectional waveguide (n_{guide}) is taken as a variable parameter, shown in Figure 3-8. It is varied from 3.377 to 3.389 in this calculation. This index variation is obtainable through carrier injection into the tuning waveguide. The distributed feedback here is assumed to be of pure gain coupling [3-8] with a coupling

coefficient of 7 cm^{-1} for mode 1 and 60 cm^{-1} for mode 2. The length of the grating section is 5 μm, and that of the nongrating section is 115 μm. Therefore the sampling interval of the grating is 120 μm, and its duty cycle is 4.2 %. We assume anti reflection (AR)-coated devices with the cavity length of 1440 μm (twelve periods of the grating-nongrating pair).

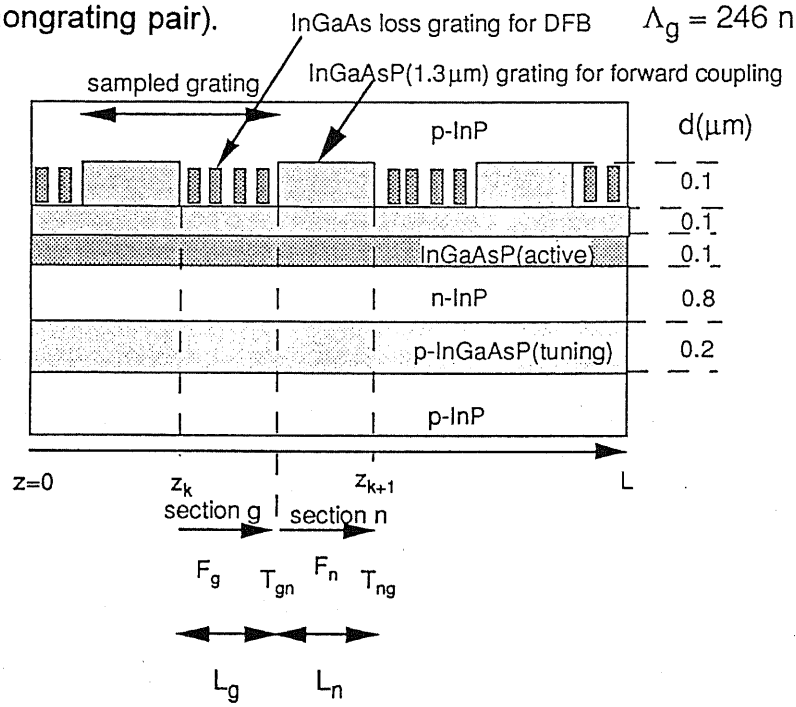

Figure 3-7 The thickness of each layer of the DFBC laser used in the simulation.

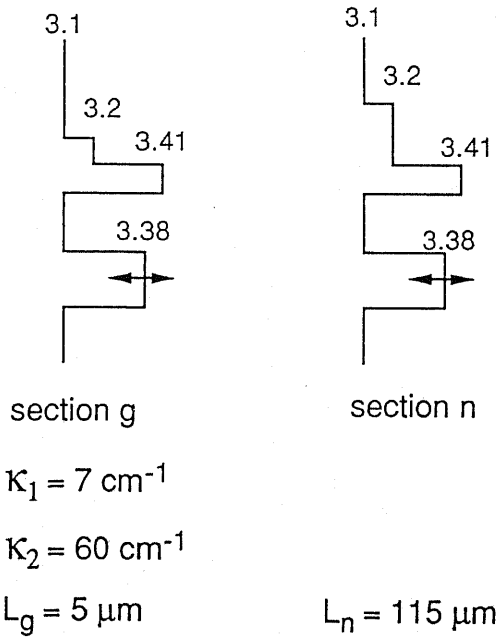

Figure 3-8 The refractive indeces and the coupling coefficients of the DFBC laser used in the simulation.

Figure 3-9 (a), (b) and (c) show calculated amplitudes of the round trip gain versus wavelength at three different refractive index values of the codirectional tuning waveguide. The spikes in these figures correspond to sampled DFB modes. The envelope on the spikes is mainly due to the codirectional forward coupling effect. the modes with the largest round-trip-gain in these figures are to become lasing modes. Since the envelope moves very fast with the index change, a wide range tuning is possible.

Figure 3-10 illustrates simulated tuning characteristics of lasing wavelength at threshold. Although the refractive index change in the codirectional tuning waveguide is small (0.01), tuning range as large as 40 nm is achieved in the figure.

Figure 3-11 shows an example of the calculated field intensity profile when the refractive index of the tuning layer is 3.383 in the same laser structure as in Fig. 2. It is understood that the light to lase sticks around the Bragg grating so as to obtain maximum feedback from the grating.

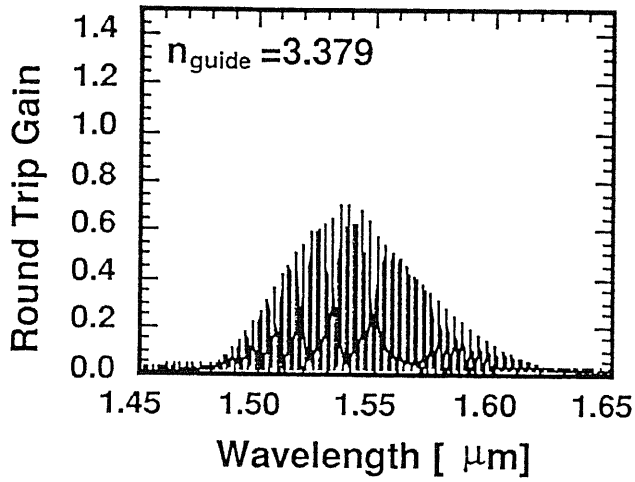

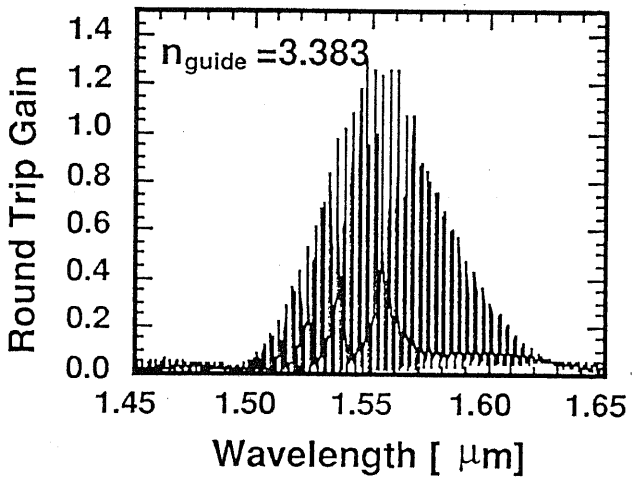

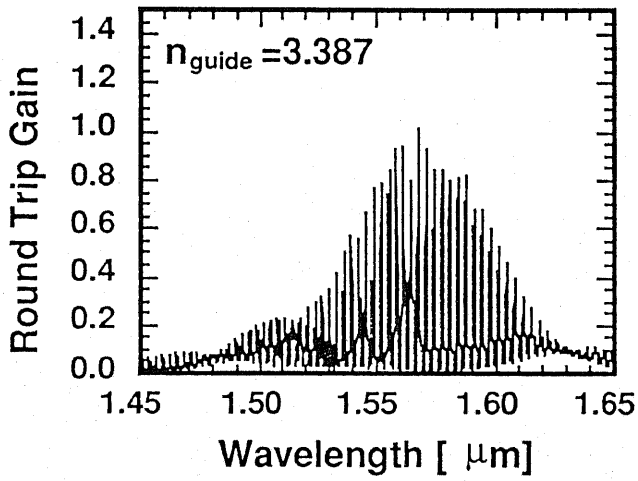

Figure 3-9 Wavelength dependence of the round trip gain in the DFBC laser with the refractive index of the codirectional waveguide layer being 3.378 (a), 3.383. (b) and 3.388 (c).

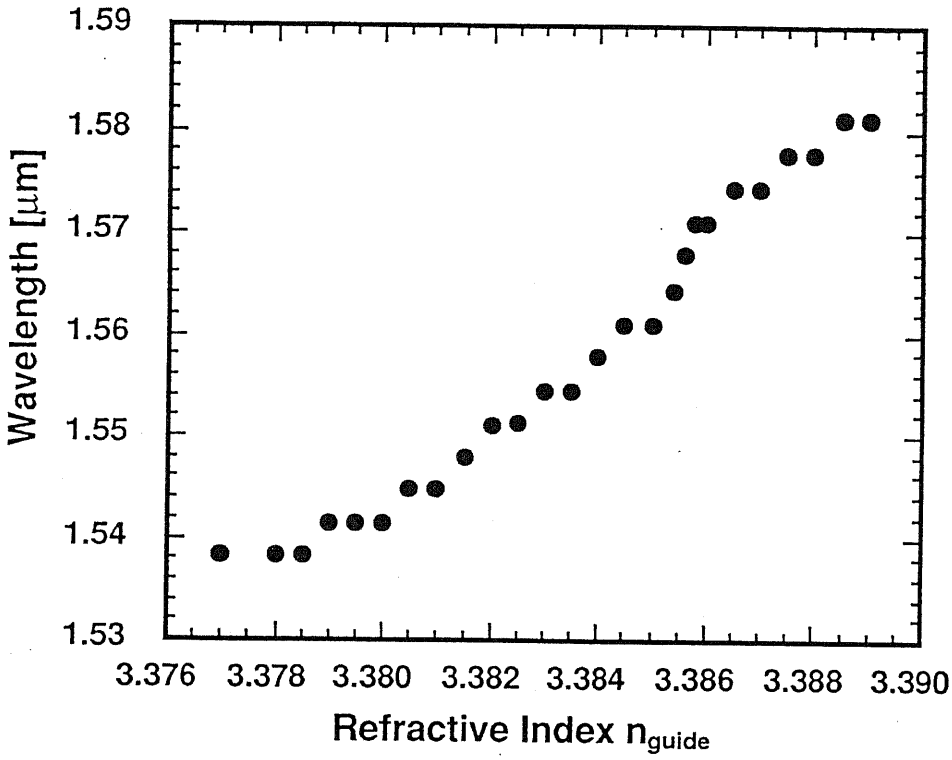

Figure 3-10 An example of simulated wavelength tuning characteristics of the DFBC laser exhibiting a tuning range over 40 nm around 1.55 μm.

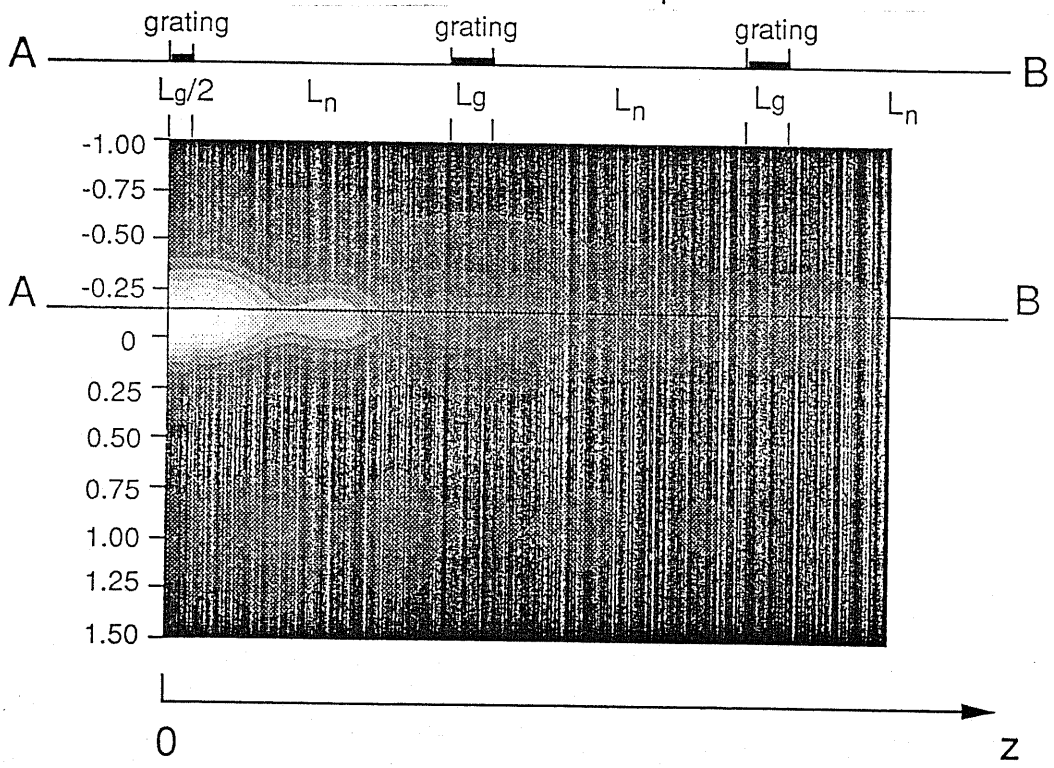

Figure 3-11 Field intensity profile of the DFBC laser. n_{guide}=3.383.

3.3.6 Discussions

In summary, we have described a new tunable laser diode, i.e., the distributed forward- and backward-coupling (DFBC) laser. This laser is characterized by a codirectional forward coupling between two parallel waveguides together with a backward distributed Bragg feedback due to sampled grating. It would provide a wide tuning range (over 40 nm, for example) as well as larger SMSR in principle compared with the other types of discontinuously-tunable laser diodes. Simple one current tuning scheme is another advantage of the DFBC laser. Either gain or index coupling, or a combination of these may be used with the DFBC laser. However, the gain coupling is preferable as it could lead to larger SMSR.

3.4 Summary

We have proposed a new type of tunable DFB laser, i.e., distributed forward- and backward-coupling (DFBC) laser and we have shown some simulation results based on two different thories. This laser is a combination of a codirectional forward coupling between two parallel waveguides together with a backward distributed Bragg feedback due to sampled grating. The filter characteristics are extremely sensitive to the change of the refractive index of one of the waveguides. The tuning range would easily be as wide as 40 nm which is used in erbium-doped fiber amplifier (EDFA) bandwidth.

We have proposed two different approaches to analyze this kind of laser, coupled-mode analyais and mode-expansion method. The mode-expansion analysis is more rigorous than the coupled-mode analysis. However, in both analyses the tuning range would be about 40 nm when the refractive index change is as little as 0.01 of one of the waveguide. Basically the former approach would be closer to the latter method when the duty cycle of the sampled grating is very small. In our simulation, the duty cycle was less than 5 %. That is why both two analyses have shown the similar results.

With these analyses, one can handle a tunable laser without Bragg grating, such as DFC lasers whose main mode is a Fabry-Perot-mode. In that case, the avarage loss in the cavity must be taken into account. On the other hand, DFBC laser has less average loss because there is less absorptive layer than DFC laser. In that sense DFBC laser is more advantageous.

Another advantage is a simple operation with only one tuning current control. Moreover, this is a kind of DFB laser, therefore the SMSR would be larger

than tunable laser with Fabry-Perot oscillator. In addition the type of gratings doesn't matter for DFBC laser, i.e., also gain-coupling grating would be acceptable, and gain-coupling grating would show more stable main mode and that would be required for the future communication networks.

References in Chapter 3

[3-1] M.-C.Amann, S. Illek, C. Schanen, and W. Thulke, "Tuning range and threshold current of the tunable twin-guide (TTG) laser," IEEE Photon. Technol. Lett., vol. 1, pp. 253-254, 1989.

[3-2] V. Jayaraman, A. Mathur, L. A. Coldren, and P. D. Dapkus, "Extended tuning range in sampled grating DBR lasers," IEEE Photon. Technol. Lett., vol. 5, pp. 489-491, 1993.

[3-3] R. C. Alferness, T. L. Koch, L. L. Buhl, F. Storz, F. Heismann, and M. J. R. Martyak, "Grating-assisted InGaAsP/InP vertical codirectional coupler filter," Appl. Phys. Lett., vol. 55, pp. 2011-2013, 1989.

[3-4] Y. Tohmori, F. Kano, H. Ishii, Y. Yoshikuni, and Y. Kondo, "Wide tuning with narrow linewidth in DFB lasers with superstructure grating (SSG)," Electron. Lett., vol. 29, pp. 1350-1352, 1993.

[3-5] M.-C. Amann, B. Borchert, S. Illek, and T. Wolf, "Widely tunable distributed forward coupled (DFC) laser," Electron. Lett., vol. 29, pp. 793-794, 1993.

[3-6] P. Vankwikelberge, G. Morthier, and R. Baets, "CLADISS ㅏ A longitudinal multimode model for the analysis of the static, dynamic and stochastic behavior of diode lasers with distributed feedback," IEEE J. Quantum Electron., vol. 26, pp. 1728-1741, 1990.

[3-7] K. Sato, G. Morthier, R. Baets, Y. Nakano, and K. Tada, "Optimum design of the grating for gain/loss coupled DFB lasers," Technical Digest of 19th European

Conference on Optical Communication (ECOC '93), Montreux, Switzerland, Tu 10, pp. 205-208, 1993.

[3-8] Y. Luo, Y. Nakano, K. Tada, T. Inoue, H. Hosomatsu, and H. Iwaoka , "Purely gain-coupled distributed feedback semiconductor lasers," Appl. Phys Lett., vol. 56, pp. 1620-1622, 1990.

[3-9] J. Willems, G. Morthier, R. Baets, "Novel widely tunable integrated optical filter with high spectral selectivity", European Conference on Optical Communication (ECOC'92), pp. 413-416, 1992.

[6]

[3-10] K. Sato, Y. Nakano, and K. Tada, "Wavelength Tuning Characteristics of Widely Tunable Distributed Forward- and Backward-Coupling Semiconductor Laser", IEEE Photon. Technol. Lett., pp. 257-259, Mar. 1995.

[3-11] H.-P. Nolting and G. Sztefka, "Eigenmode Matching and Propagation Theory of Square Meander-Type Couplers", IEEE Photon. Technol. Lett., vol. 4, pp. 1386-1389, Dec. 1992.

Chapter 4 Parameter extraction of DFB laser diodes

4.1 Introductory remarks -- Why is it so difficult for GC-DFB lasers?

In this chapter we describe that gain and index coupling coefficients in cleaved DFB laser diodes has successfully been determined by fitting theoretical subthreshold spectra to experimentally observed ones. Other parameters including gain and group index as well as their dispersion are extracted simultaneously.

Determination of device parameters in fabricated distributed feedback (DFB) laser diodes is very important for further optimisation of the laser design and even the system design. In particular, the coupling coefficient is one of the most influential parameters, and hence should be measured precisely. However, the determination of the coupling coefficient in DFB lasers so far was only possible for index-coupled devices with antireflection-coated (AR-coated) facets, and it was not very accurate [4-1]. Moreover, in such measurements, no other parameters such as gain and effective group index could be derived.

There is a big problem especially for the determination of the gain-coupling coefficients. As shown in Figure 4-1, the determination of index-coupling coefficients is not difficult because it is observed as the stop-bandwidth of AR-coated index-coupling laser [4-1]. On the other hand, gain-coupling coefficient is observed as gain parameter in Figure 4-2, therefore it is very difficult to extract gain-coupling coefficient from the gain parameter. Moreover, one should have known the material parameters, such as refractive index etc., however the difference between the designed values and actual values is not very small. Here we propose a new approach to determine accurately index- and gain-coupling coefficients, reflectivities at both facets, phase of the grating at the facets, gain, effective index, and even

linewidth enhancement factor.

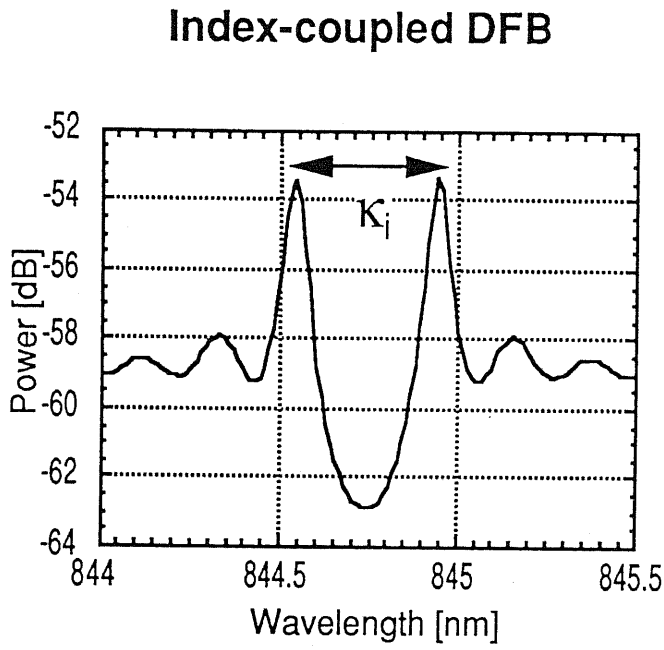

Figure 4-1 Spectrum of purely index-coupled DFB laser with AR-coated at both facets.

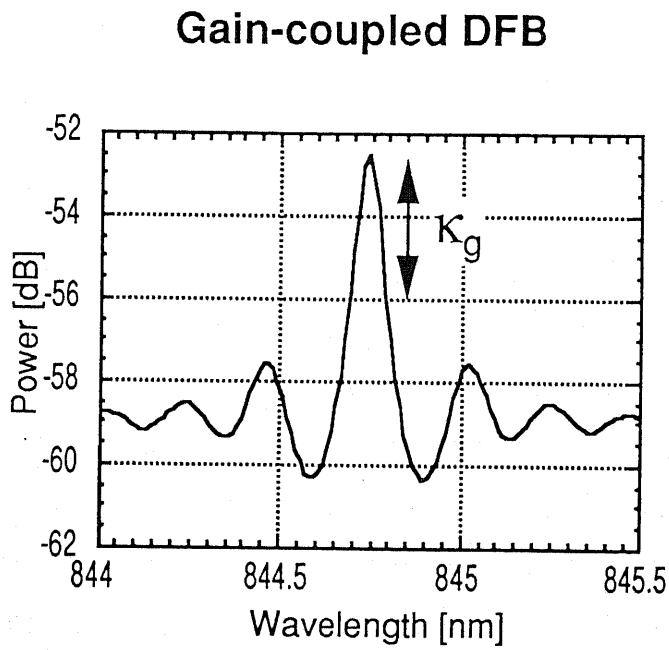

Figure 4-2 Spetctrum of purely gain-coupled DFB laser with AR-coated at both facets.

4.2 Curve-fitting method

The method we propose here, the numerical fitting of subthreshold spectra to well-known analytical (be it rather complicated) expressions [4-2] , allows us to determine the coupling coefficient as well as refractive index, gain, and their dispersion very accurately. Furthermore, the method is applicable to DFB laser diodes with both index and gain coupling.

The analytical expression for the spectrum is based on the transfer matrix method as has been described in Reference [4-2]. It is also assumed that the spontaneous emission has no influence on the carrier density, which implies that the fitting must be done on spectra that are measured at sufficiently low current below threshold. In principle, this method is very general and allows different functional dependencies to be included. It can also be applied to multiple section lasers or lasers with nonuniform gratings (e.g. for tuning). By applying the fitting to spectra obtained at different currents, one can also determine the differential gain and the linewidth enhancement factor.

$$P_{spon}=\frac{J_{sp}}{2}\int_0^L \frac{|trans|^2(1+|r|)^2}{|1-rnd|^2}dz \qquad (4\text{-}1),$$

where J_{sp} is spontaneous emission rate, and the spontaneous emission is amplified along the cavity and observed at the right facet. This expression is derived as a sum of the infinite series of the amplfied spontaneous emission. The spontaneous emission is generated along the cavity, therefore the integral of the local spontaneous emission results in the total spontaneous emission power. As shown in (4-1), rnd is the round-trip-gain at the coordinate z, ρ is the reflectivity of the left

laser cavity at the coordinate z, and trans is the transition rate of the right laser cavity. These are expressed with elements of F-matrix, and functions of the various parameters of semiconductor laser diodes. For instance, gain, effective refractive index, and reflectivities at both facets are expressed as follows,

$$g=g_0-g_1(E(\lambda)-E_p)^2 \qquad (4\text{-}2)\ (a)$$

$$n_{eff}=n_g-\frac{dn_{eff}}{d\lambda}\lambda+n_2\lambda^2+n_3\lambda^3 \qquad (4\text{-}2)\ (b)$$

$$\rho_1=R_1\exp(j\psi_1) \qquad (4\text{-}2)\ (c)$$

$$\rho_2=R_2\exp(j\psi_2) \qquad (4\text{-}2)\ (d),$$

where g is gain in the active layer and is assumed to be a quadratic function of the photon energy E, g_0 is the peak gain, g_1 is the gain curvature, and E_p is the peak gain. In equation (4-2) (b), effective refractive index is dependent on the wavelength. In equations (4-2) (c) and (d), the reflectivities are devided into two terms, such as the amplitude of the reflectivity and the phase.

Therefore the number of the parameters used here is 14, such as, J_{sp}, g_0, g_1, E_p, n_g, n_2, n_3, $dn_{eff}/d\lambda$, reflectivities R_1, R_2, phase φ_1, φ_2, index-coupling coefficient κ_i, gain-coupling coefficient κ_g, and the coupling efficiency from the laser to the fiber which is connected to the experimental setup.

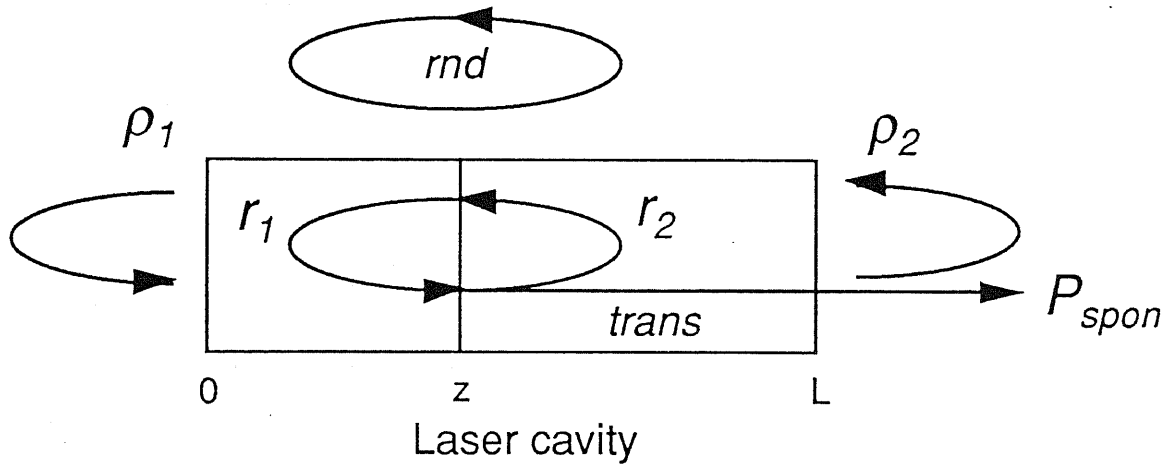

Figure 4-3 Spontaneous emission in the laser cavity.

4.3 Fitting procedure

We have implemented the method for single section lasers with both index and gain coupling, assuming a constant spontaneous emission rate, but a linear dependence of refractive index on wavelength and a quadratic dependence of gain on photon energy. The numerical fitting was based on minimisation of the sum of the squared differences between modelled and measured results using a standard optimisation routine [4-3]. Here we show the fitting procedure.

1. Measurement of subthreshold spectrum and the cavity length.

2. Estimate initial values of gain and effective refractive index.

Also rough estimation of $g(\lambda)$ and $n(\lambda)$ from the FP spectrum.

3. Estimate initial values of coupling-coefficients and the phase of the grating.
   Index-coupling coefficient is roughly estimated from the DFB spectrum.

4. Computation

5. Error assessment
   The change of the parameters is estimated if the sum of the squared differences change in 1 %.

6. Estimation of linewidth enhancement factor.
   From two parameter sets fitted fromthe spectra at the different bias.

In this curve-fitting method, the most important thing is that the estimation of the initial values must be very properly performed.

4.4 Measurements and iffting results

The fitting has been done for several MQW AlGaAs/GaAs gain-coupled DFB lasers [4-4] with cleaved facets, a cavity length of 200 μm, and a grating period of 373.9 nm (third order) as shown in Figure 4-4. Two examples of measured and fitted spectra for lasers (labeled 202, 2003, and g05b) from different wafers are shown in Figure 4-5. We have used logarithmic spectra since the stop band is as important in the fitting as the mode resonances. The span was carefully chosen to include a few Fabry-Perot resonances from which gain and group index could be estimated very easily. Because the lasers are as cleaved at both facets, the

reflectivities are fixed to be 0.5657, and refractive index coefficients n_2 and n_3 equal to be 0. Therefore the number of the parameters is reduced to be 10.

The index and gain coupling coefficients are found to be 26.6 and 7.3 cm $^{-1}$ for Figure 4-5 (a), respectively, and 59.2 and 23.4 cm $^{-1}$ for Figure 4-5 (b). Among lasers from the same wafer, a good agreement of the coupling coefficients was found. A summary of the extracted device parameters is given in Table I.

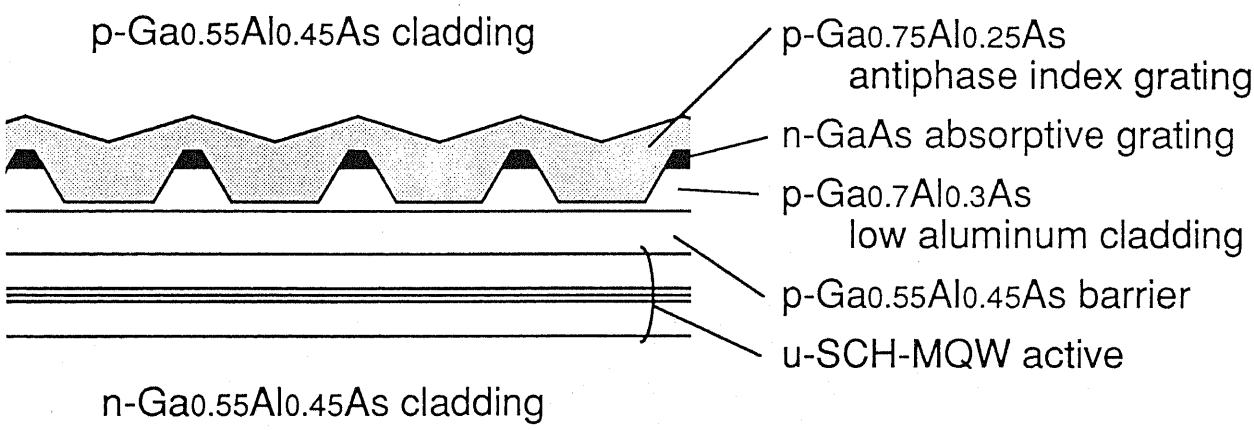

as-cleaved: R_1, R_2 ← fixed

$$n_{eff} = n_g - \frac{dn_{eff}}{d\lambda}\lambda$$

Figure 4-4 Schematic longitudinal cross section ot gain-coupled DFB laser which was used for the measurement.

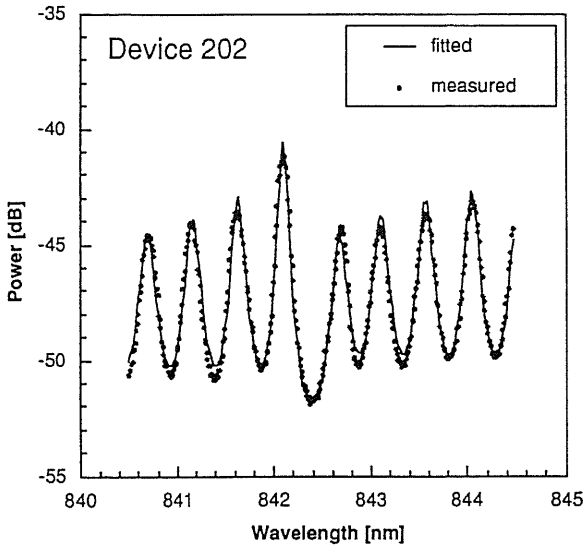

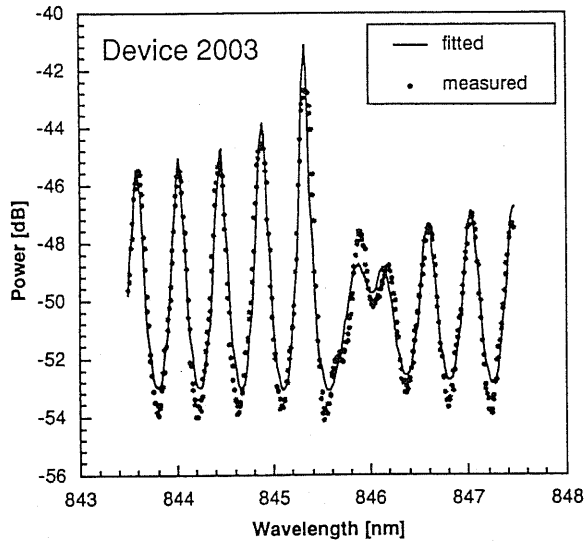

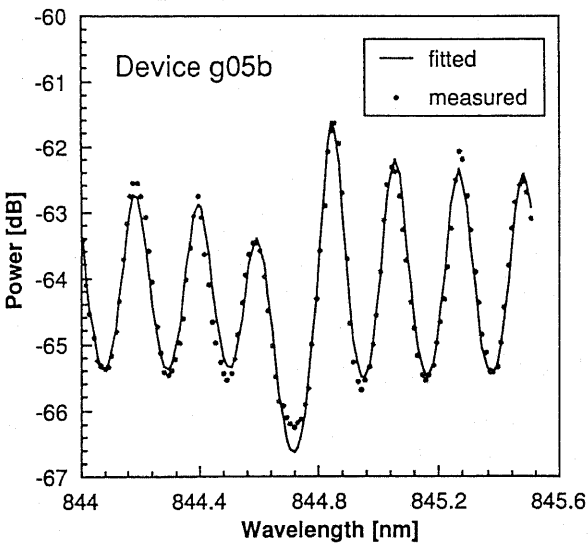

Figure 4-5 Measured (--) and fitted (·) spectra for three cleaved gain coupled DFB lasers. (a) device 202, (b) device 2003, and (c) device g05b.

parameter [unit]	Dev. 202	Dev. 2003	Dev. g05b
Cavity length (L) [μm]	195	210	400
Index coupling (κ_i) [cm^{-1}]	27.2 ±1.4	56.4 ±3.0	10.1 ±0.5
Gain coupling (κ_g) [cm^{-1}]	7.5 ±1.0	22.3 ±2.5	4.3 ±0.5
Peak gain - absorption (g_0-α_{int}) [cm^{-1}]	146 ±14	101 ±10	24.1 ±2.4
Peak energy (E_p) [eV]	1.467±0.001	1.466±0.001	1.476±0.001
Gain curvature (g_1) [$cm^{-1}eV^{-2}$]	-297	-161	-11.2
Group index (n_g)	3.82 ±0.	3.94 ±0.	4.15 ±0.
$dn_{eff}/d\lambda$ [μm^{-1}]	-0.52 ±0.	-0.65 ±0.	-0.90 ±0.
Left facet phase (ψ_1) [rad.]	-0.75 ±0.01	0.36 ±0.01	1.41 ±0.01
Right facet phase (ψ_2) [rad.]	-2.84 ±0.02	0.98 ±0.01	-0.47 ±0.01

Table I Device parameters extracted from the subthreshold spectra.

4.5 Error assessment

In this section we disscuss he sensitivity of each extracted parameter to evaluation function. The errors in Table I are the values that give 1 % increase of the evaluation function. As shown in Figure 4-6, each parameter has the deviation from the calculated value when the evaluation function increases 1 %. In Table I, gain-coupling coefficient shows more error than index-coupling coefficient.

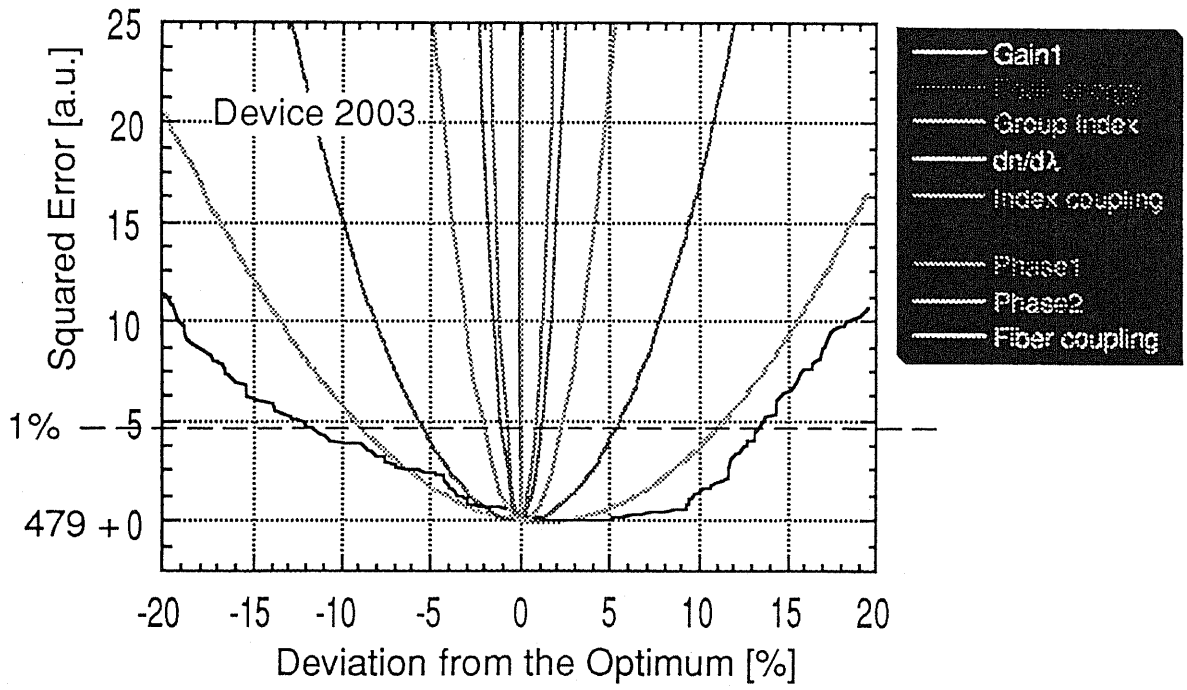

Figure 4-6 Squared error of each laser parameter extracted by curve-fitting. The horizontal dotted-line shows the limit of 1 % increase of the evaluation function.

4.6 Extracting linewidth enhancement factor

Linewidth enhancement factor can be also determined by this curve-fitting method. In Figure 4-7, we show the L-I characteristics of device g05b. The threshold current is 24 mA, and the curve-fitting was performed for the spectra at 23 and 24 mA bias current. We have estimated linewidth enhancement factor with the extracted parameters and an equation,

$$\alpha = -\frac{4\pi}{\lambda}\frac{dn_{re}/dN}{dn_{im}/dN} \qquad (4\text{-}3),$$

then we obtained linewith enhancement factor of 2.5.

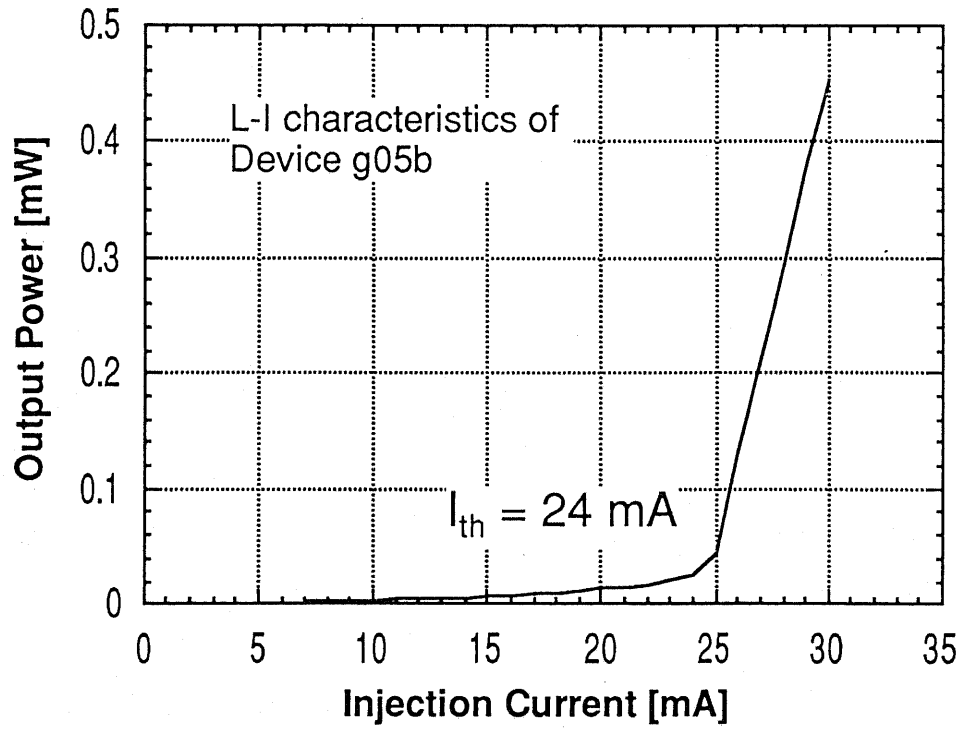

Figure 4-7 L-I characteristics of gain-coupled DFB laser. Device g05b.

4.7 Summary

It is concluded that excellent agreement between theoretical and experimental spectra is obtained in spite of the possible non-uniformities in the devices and in spite of the rough approximations for gain and spontaneous emission. In some cases, a better agreement could probably be reached if we used a wavelength dependent spontaneous emission rate and/or a wavelength dependence of the gain that is more suited for quantum wells than the parabolic function used here. In order to apply this method for DFBC lasers, one should impliment multi-section and multi-mode analysis. This is a futher investigation of this study.

Appendix Determination of GC coefficient with an approximated function.

We discuss a roughly estimation of gain-coupling coefficient with an approximated function. We have developed a similar method to the estimation of index-coupling coefficients in reference [4-1]. The spectrum of spontaneous emission is influenced when the gain-coupling coefficient changes. Normally the gain parameter changes, however the full-width-half-maximum (FWHM) of the gain spectrum is also changed. Therefore we derived the equation from carrier rate-equation.

$$-v_g(\Gamma g-\alpha_{int}-2\alpha_{end}+2\kappa_g f_{st})=\frac{R_{sp}}{I}=\frac{2\pi\Delta v}{K} \qquad (4\text{-}4),$$

where v_g is the group velocity of light, Γ is the confinement factor of light, α_{int} is internal loss, aend is facet loss f_{st} is the standing wave factor [4-5], R_{sp} is spontaneous emission rate, I is photon number, and K is Petermann's K-factor [4-6]. Here the laser is almost index-coupled and relatively small gain-coupled, then the stop band is clearly observed, and we assume identical material gain, facet loss, and K-factor. Therefore we can estimate gain-coupling coefficients with this equation,

$$\kappa_g=\frac{\pi^2}{8v_g}(\Delta v_{i+1}-\Delta v_i) \qquad (4\text{-}5)$$

We applied this equation for a gain-coupled DFB laser. Figure 4-8 shows a spectrum of a gain-coupled DFB laser with bulk active layer and loss grating. Here

we obtained gain-couling coefficient κ_g=13.6 cm^{-1}, and index-coupling coefficient κ_i=87.5 cm^{-1}. Although this is an approximation, it is good for a rough estimation.

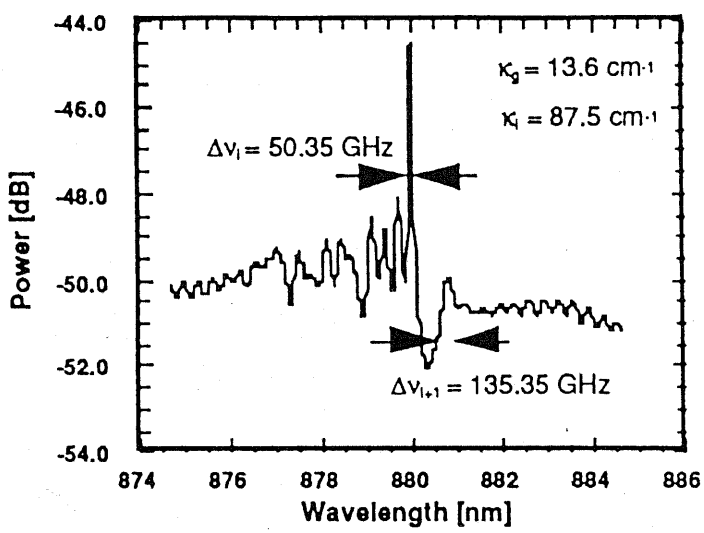

Figure 4-8 A spectrum of an AR-coated gain-coupled DFB laser.

References in Chapter 4

[4-1] L. J. P. Ketelsen, I. Hoshino, and D. A. Ackerman, "Experimental and Theoretical Evaluation of the CW Suppression of TE Side Modes in Conventional 1.55 um InP-InGaAsP Distributed Feedback Lasers", IEEE J. Quantum Electron., vol. 27, pp. 965-975, April 1991.

[4-2] T. Makino and J. Glinski, "Transfer Matrix Analysis of the Amplified Spontaneous Emission of DFB Semiconductor Laser Amplifiers", IEEE J. Quantum Electron., vol. 24, pp. 1507-1518, Aug. 1988.

[4-3] J. E. Dennis, D. M. Gay, and R. E. Welsh, "An Adaptive Nonlinear Least-Squares Algorithm", ACM Trans. Math. Software, Vol. 7, No. 3 (1981).

[4-4] Y. Nakano, H. L. Cao, K. Tada, Y. Luo, M. Dobashi, and H. Hosomatsu, "Absorptive-grating gain-coupled distributed-feedback MQW lasers with low threshold current and high single-longitudinal-mode yield", Jpn. J. Appl. Phys. 32, pp. 825-829, Feb. 1993.

[4-5] R. Baets, K. David, and G. Morthier, "On the distinctive features of gain-coupled DFB lasers and DFB lasers with second-order grating", IEEE J. Quantum Electron., vol. 29, pp. 1792-1798, June 1993.

[4-6] J. Wang, N. Schunk, and K. Petermann, Electron. Lett., vol, 23, pp. 715-717, July 1987.

Chapter 5 Design of DFBC lasers

5.1 Introductory remarks

In this chapter we design the DFBC structure of 0.84 μm wavelength scheme, i.e., GaAs/AlGaAs material system. Therefore the material parameters we use here are for GaAs/AlGaAs DFBC laser diodes. There are five design steps as follows,

1. waveguide
2. layer structure
3. electrodes
4. photo-masks
5. process

In order to simplify the process, we designed this particular layer structure with which only one regrowth step is required. we describe each step in this chapter.

5.2 Design of waveguides

We have already described in Chapter 3 that DFBC laser has two eigen modes because of the codirectional waveguide. Therefore the waveguide shold be designed carefully in order to realize a good wavelength filter which scrambles the eigen modes. In addition one of the two eigen modes should have larger gain and larger Bragg reflection from the Bragg gratings. Figure 5-1 (a) and (b) show the amplitude of the eigen modes in the waveguides of DFBC lasers.

In the Bragg grating section (Figure 5-1 (a)), the even mode is almost confined in the active layer and fed back more from the Bragg grating. On the other hand, the odd mode is almost confined in the codirectional waveguide (tuning layer), and fed back less from the Bragg gratings. Generally the fundamental mode (here odd mode) has the largest effective refractive index, therefore it could be confined in the active layer. However here the thickness of the active layer is rather thinner, and the thickness of the codirectional waveguide is rather thicker. Therefore the fundamental mode is confined in the codirectional waveguide in which the effective refractive index is larger than in the active layer.

In the non-Bragg grating section (Figure 5-1 (b)), both two eigen modes propagate and obtain almost the same amount of gain from the active layer. The total power of light propagates zig-zag along the laser cavity and the period of the forward coupling length is about 100 μm for this particular structure.

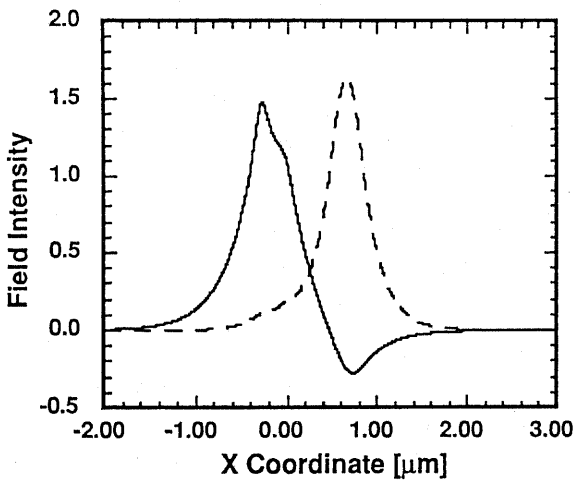

ブラッググレーティングのある区間

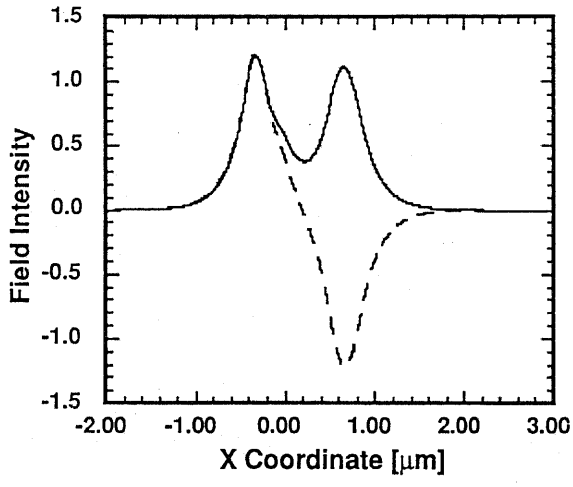

ブラッググレーティングのない区間

Figure 5-1 The eigen modes of the DFBC laser, which are calculated with the designed waveguides. (a) Bragg-grating section and (b) non-Bragg grating section.

5.3 Design of layer structure

The refractive index and the thickness of each layer are designed as shown in Figure 5-2 to provide the eigen modes as described in section 5.2. In order to reduce the regrowth steps, we designed the structure as simple as possible. As shown in Figure 5-2, this particular device requires only one regrowth step. Generally for the tunable lasers with lateral current injection such as TTG lasers [5-1], more than three regrowth steps are required. As shown in Figure 5-2, n-clad, tuning layer, spacer and active layer are grown in the first growth stemp. After the first cristal growth, sampled grating is formed by chemical etching, then the regrowth step makes the upper-clad and the cap layer.

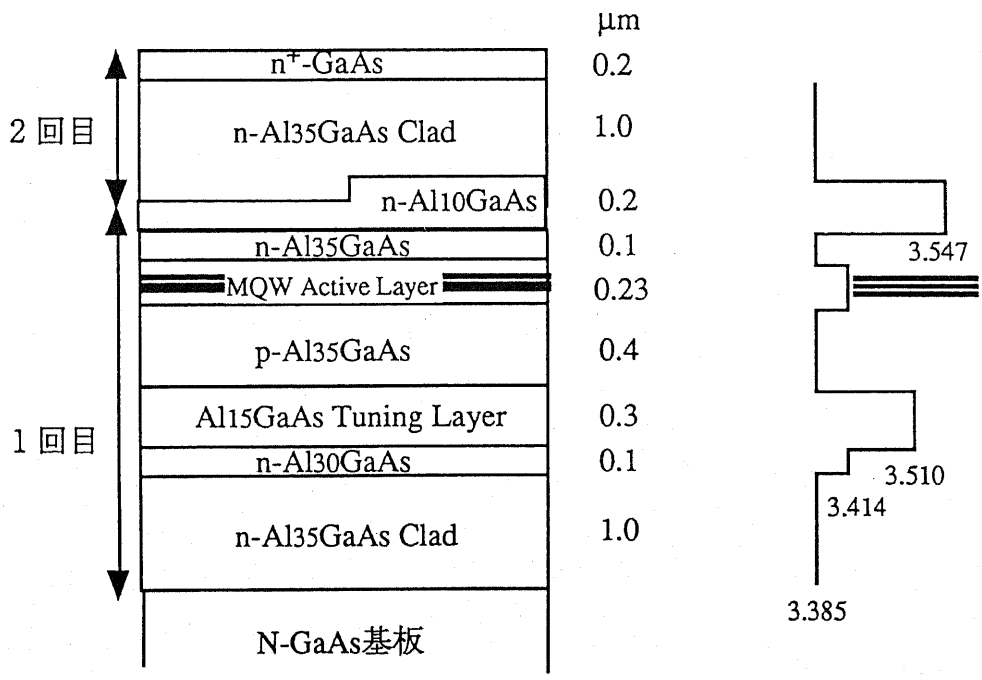

Figure 5-2 The designed layer structure of the DFBC laser.

5.4 Design of electrodes

DFBC laser diodes have a tuning layer, and the refractive index of the tuning layer must be changed independently with the lateral control current injection. The cross section of our particular device is shown in Figure 5-3, and the p-electrode is located simply beside the n-electrode. However the light propagates almost just under the n-electrode, and the tuning current goes through just under the p-electrode. Therefore for this particular device, the distance between the waveguide and the tuning layer cannot be very short. In order to make the processing tolerance high, this distance must be more than 10 μm. Then we use LASTIP (carrier-flow analyzer) to estimate the carrier concentration as a function of the distance from the center of the p-electrode. This program LASTIP analyzes the current flow with finite element method. andFigure 5-4 shows the simulation result. In Figure 5-4, at the distance of 20 μm, the carrier concentration in the tuning layer is 1.3 X 10^{17} cm^{-3} at 10 mA bias, which means 1.7X10^{-4} refractive index change [5-2]. 20 μm is desirable because the refractive index change is not very small, and the process tolerance is still very high. For 20 μm distance, the tuning range would be about 4 nm for 0.84 μm wavelength scheme.

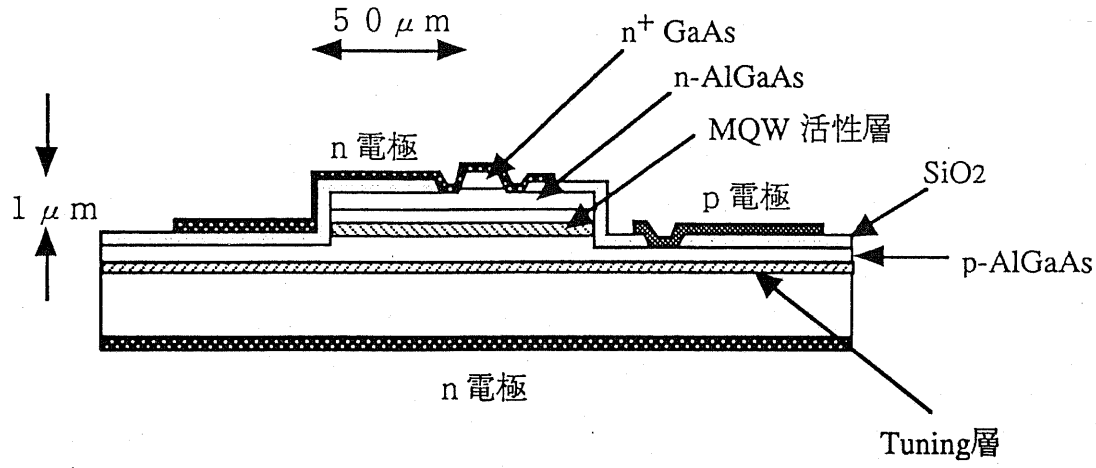

Figure 5-3 A designed schematic lateral cross section of the DFBC laser.

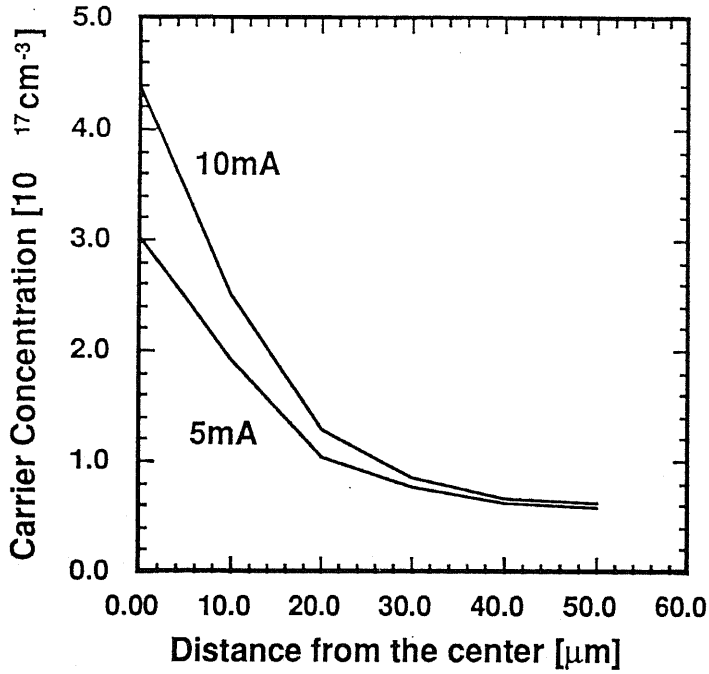

Figure 5-4 A simulation of the carrier concentration as a function of the distance from the center of the p-electrode, calculated with LASTIP.

5.5 Design of photo-masks

We show the picture of our photo-masks which are used for the process. In the next chapter we show the process proceedure, however here we show only the name of the masks.

1. sampled grating
2. laser stripe pattern
3. mesa etching pattern
4. p-type electrode contact hole
5. p-type electrode pad
6. n-type electrode contact hole
7. n-type electrode pad
8. 7 degrees tilted edge

In Figure 5-5 (a) and (b) we show the picture of the masks. At each process step we have 5 μm process tolerance.

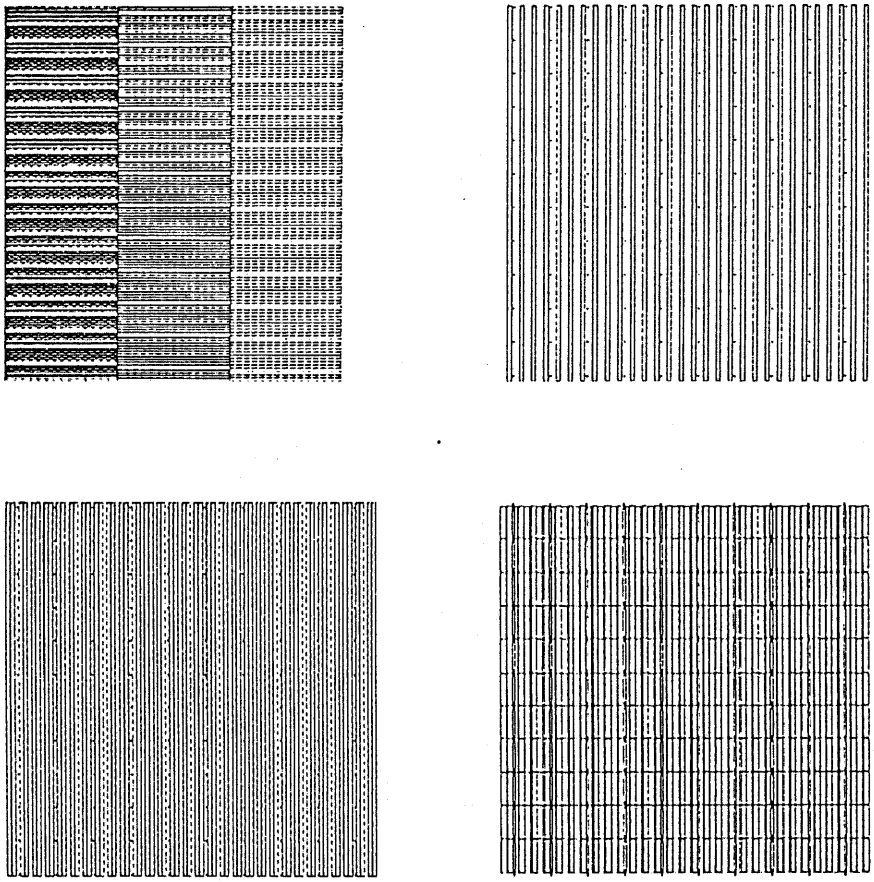

Figure 5-5 Pictures of the photo-masks used in the fabrication process of the DFBC laser. (a) sampled grating, p-type electrode pad, n-type electrode pad, 7 degrees tilted edge.

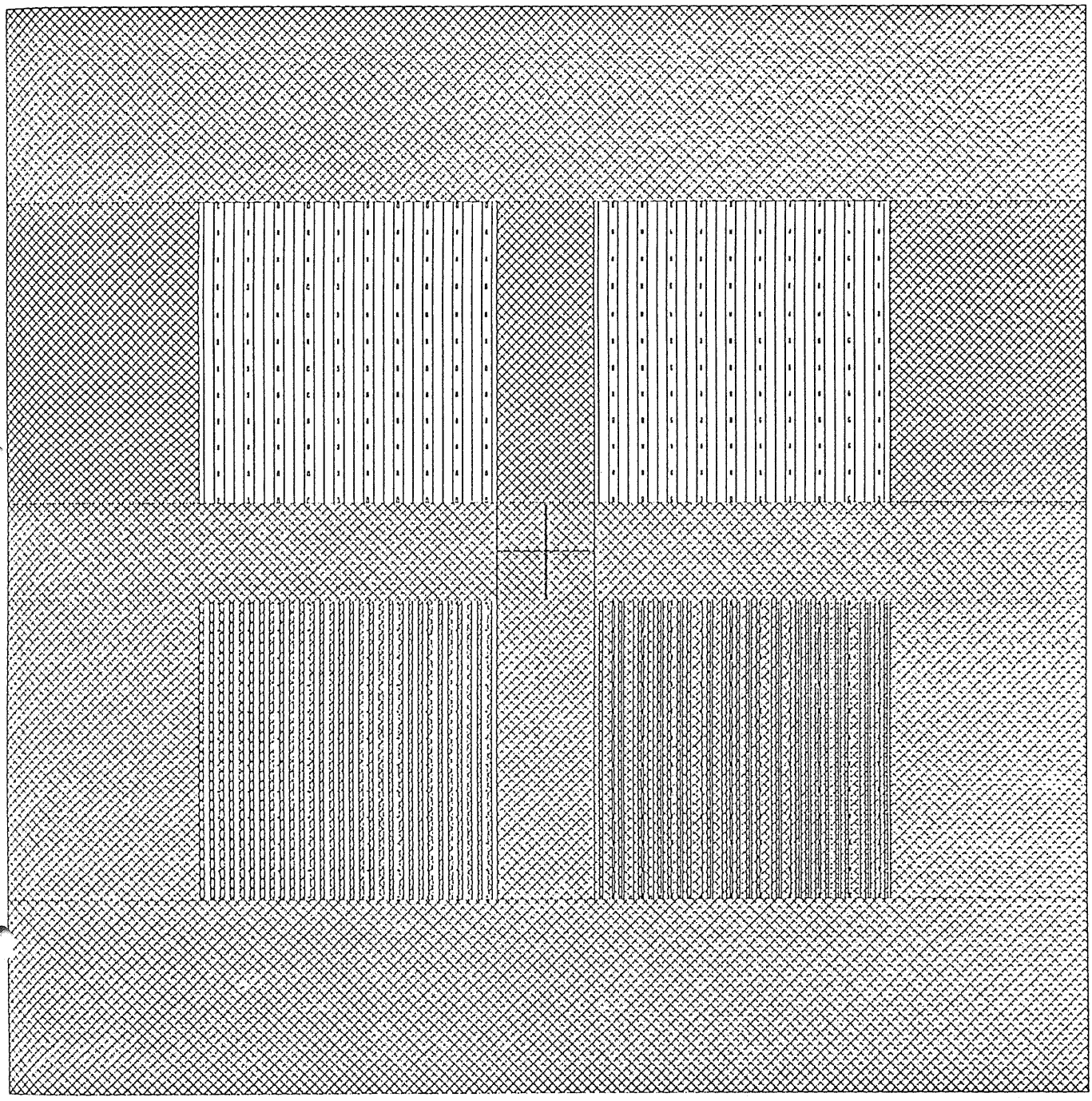

Figure 5-5 Pictures of the photo-masks used in the fabrication process of the DFBC laser. (b) laser stripe pattern, mesa etching pattern, p-type electrode contact hole, n-type electrode contact hole.

5.6 Design of process

Here we show our process procedure to fabricate DFBC lasers in Figure 5-6. The process is devided roughly into eleven steps.

1. first epitaxial growth	
2. making sampled grating	mask #1
3. regrowth step	
4. making laser stripe	mask #2
5. making mesa pattern	mask #3
6. SiO_2 deposition	
7. etching p-type contact hole	mask #4
8. evaporating AuZn	mask #5
9. etching n-type contact hole	mask #6
10. evaporating AuGe	mask #7
11. etching 7 degrees titled edge	mask #8

Figure 5-6 Process procedure to fabricate DFBC laser diodes.

使用するレジストはすべてポジ
図中のマスク下面にはパターンが書かれてあります。

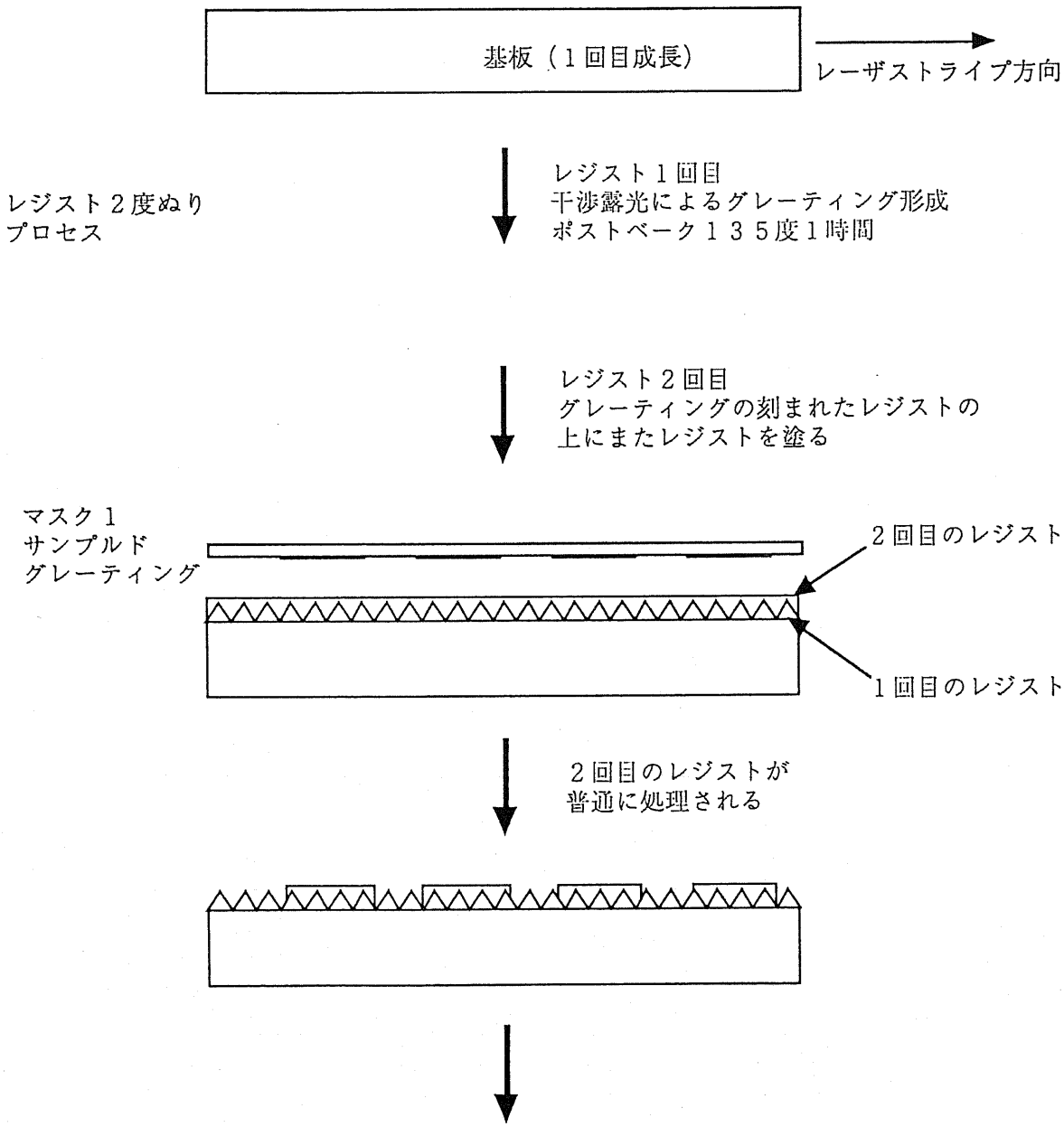

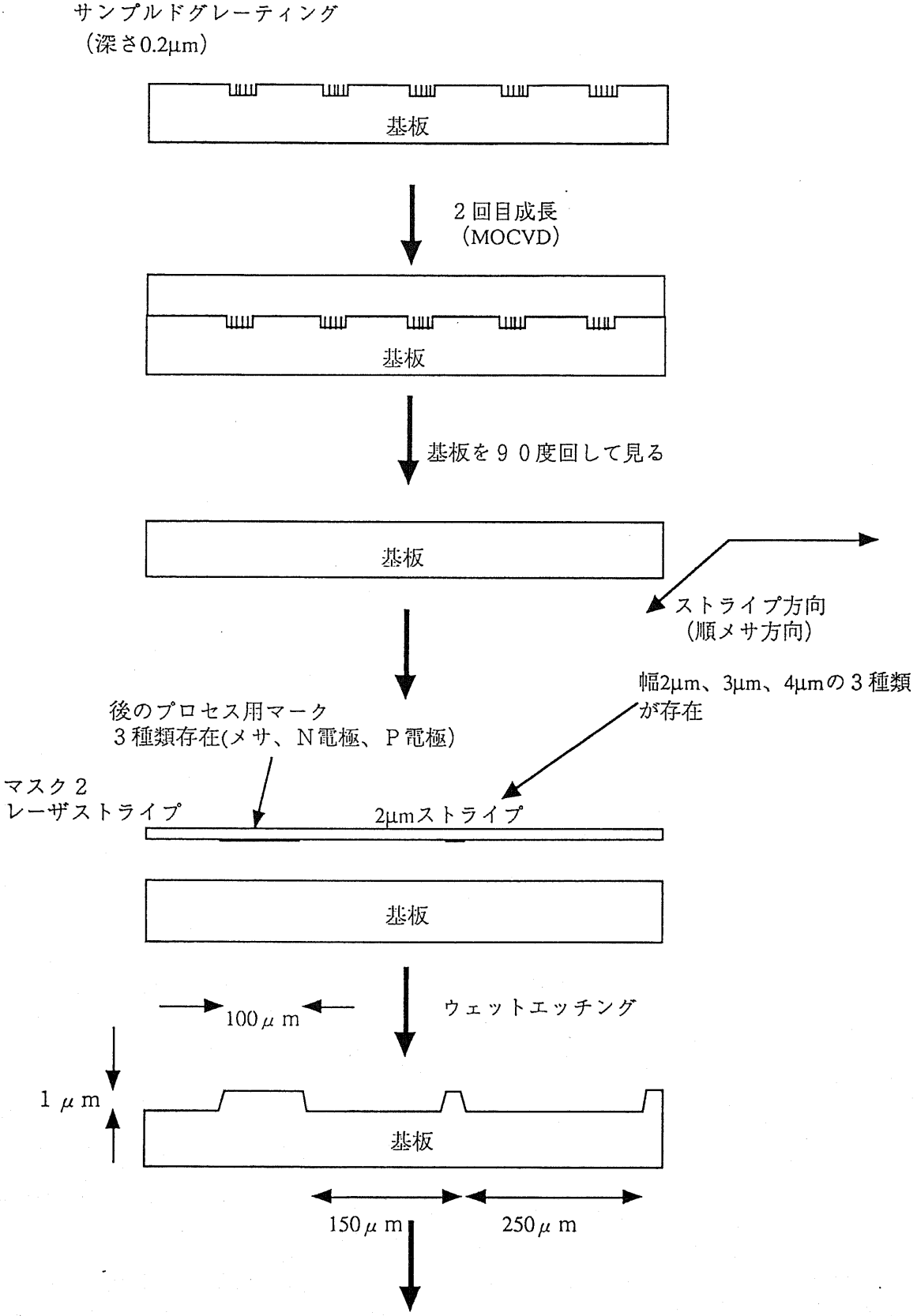
サンプルドグレーティング
（深さ0.2μm）
基板
2回目成長
（MOCVD）
基板
基板を９０度回して見る
基板
ストライプ方向
（順メサ方向）
幅2μm、3μm、4μmの３種類
が存在
後のプロセス用マーク
３種類存在(メサ、Ｎ電極、Ｐ電極)
マスク２
レーザストライプ
2μmストライプ
基板
100μm
ウェットエッチング
1μm
基板
150μm
250μm

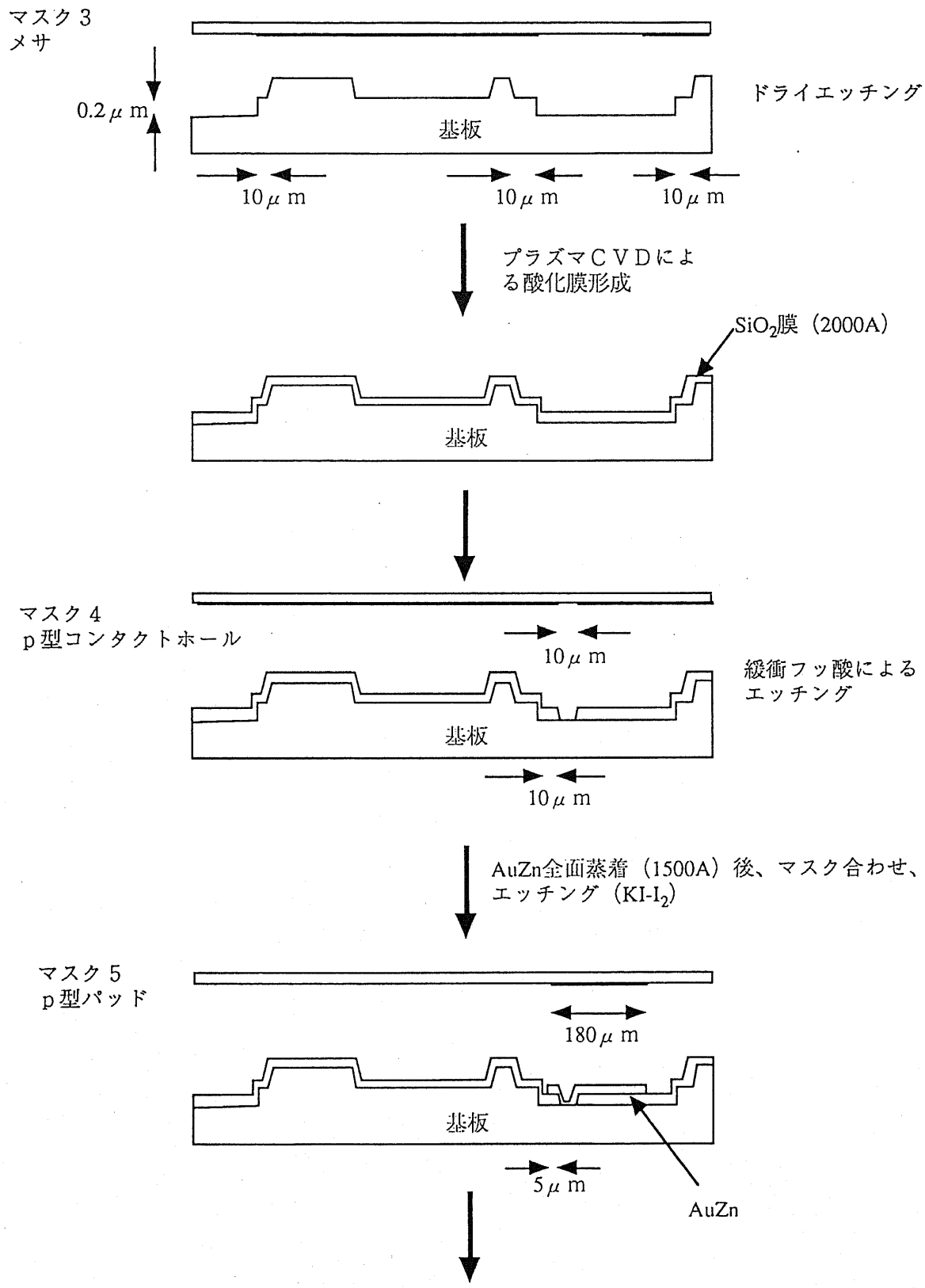
マスク３
メサ
0.2μm
基板
10μm
10μm
10μm
ドライエッチング
プラズマＣＶＤによる酸化膜形成
SiO_2膜（2000A）
基板
マスク４
ｐ型コンタクトホール
10μm
基板
10μm
緩衝フッ酸によるエッチング
AuZn全面蒸着（1500A）後、マスク合わせ、エッチング（$KI-I_2$）
マスク５
ｐ型パッド
180μm
基板
5μm
AuZn

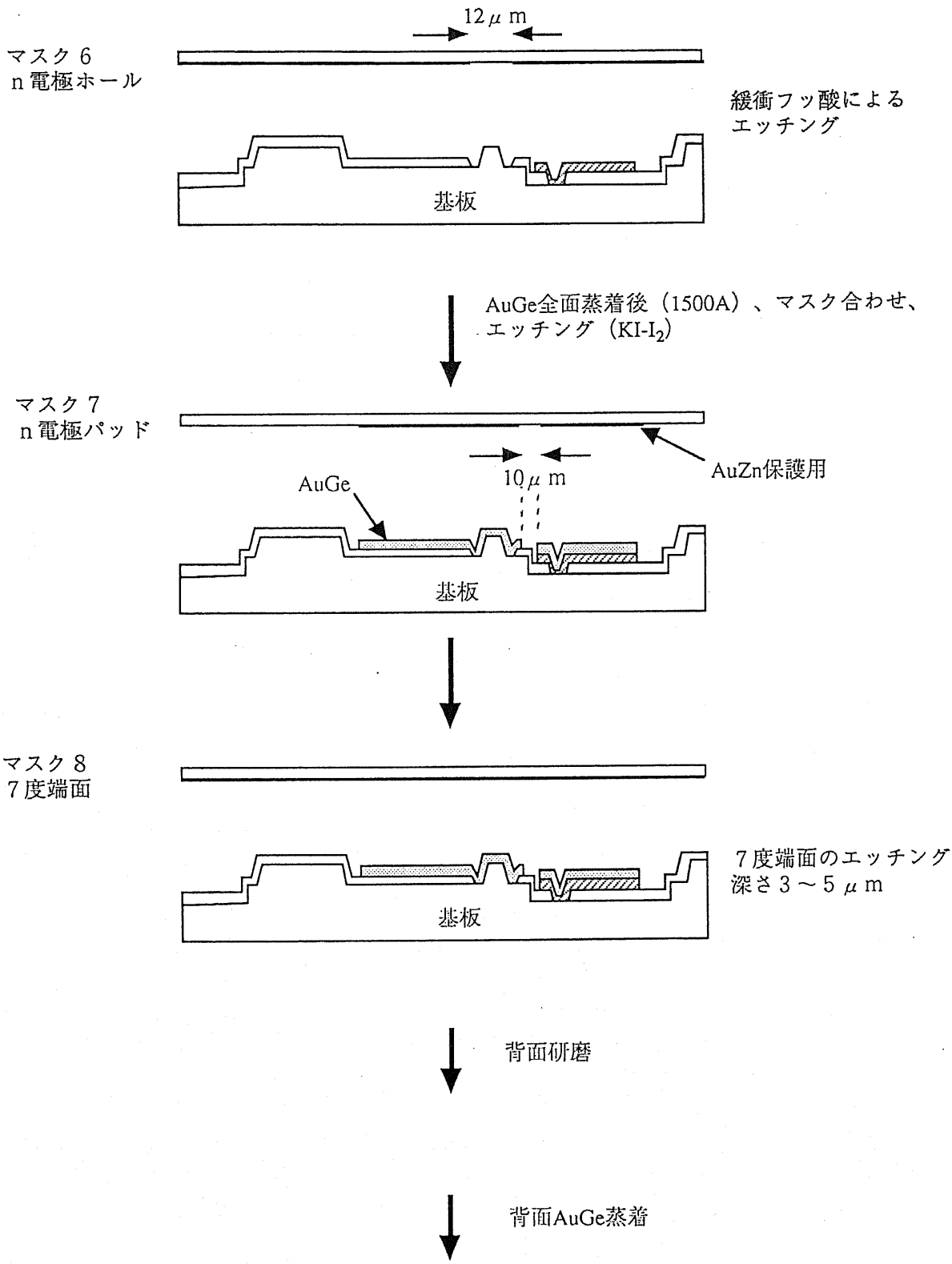
12μm
マスク6
n電極ホール
緩衝フッ酸による
エッチング
基板
AuGe全面蒸着後（1500A）、マスク合わせ、
エッチング（KI-I2）
マスク7
n電極パッド
AuZn保護用
10μm
AuGe
基板
マスク8
7度端面
7度端面のエッチング
深さ3～5μm
基板
背面研磨
背面AuGe蒸着

5.7 Summary

In this chapter we describe the four steps of the structure design. This particular device needs only one regrowth step, however needs eight photo-masks. The distance between the p-electrode and the n-electrode is designed to be 20 μm in order to make the process tolerance high. For this design, the refractive index change in the tuning layer is still big and the tuning range would be 4 nm for 0.84 μm wavelength scheme. Our photo-masks are designed in order to simplify the process steps, however we need still eight masks. Each step is designed for higher process tolerance such as 5 μm error.

References in Chapter 5

[5-1] M.-C.Amann, S. Illek, C. Schanen, and W. Thulke, "Tuning range and threshold current of the tunable twin-guide (TTG) laser," IEEE Photon. Technol. Lett., vol. 1, pp. 253-254, 1989.

[5-2] S. Adachi, "Physical Properties of III-V Semiconductor Compounds", John Wiley & Sons, pp. 189-182, 1992.

Chapter 6 Fabrication of DFBC lasers

6.1 Introductory remarks

In this chapter, we show experimental results of fabricating DFBC lasers. As described in Chapter 5, we have two epitaxial growths and seven photo-lithographies. Here we make DFBC lasers of GaAs based material with 840 nm wavelength, therefore all the process was done on GaAs wafer.

6.2 First epitaxial growth

At first, an epitaxial growth on a GaAs-wafer was done by metal-organic chemical vapor deposition (MOCVD). Figure 6-1 shows the scanning electron microscope (SEM) photograph of the cross section of the wafer after the first epitaxial growth. Each layer is grown in the way of the design.

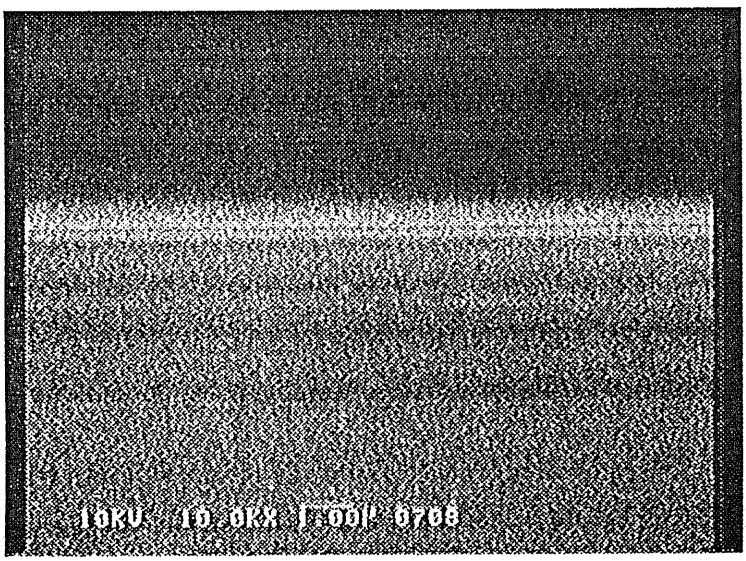

Figure 6-1 Scanning electron microscope photograph of cross section of the wafer after the first epitaxial growth.

In order to make sure if the active layer was preferably grown, we have measured photo-luminnescence of the wafer. It is shown in Figure 6-2.

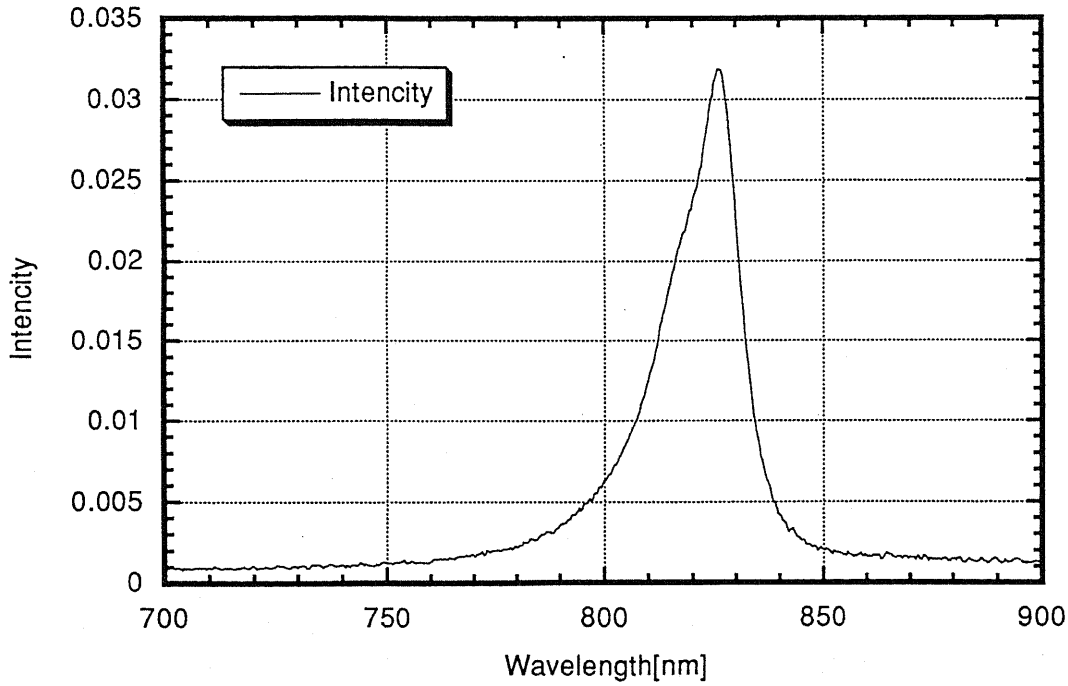

Figure 6-2 Photo-luminescence of the wafer after the first epitaxy.

6.3 Making sampled grating

In order to make a sampled grating, we should know etching rate of AlGaAs wafer. We used ECR-RIBE for this purpose, and we measured the dry etching rate. Figure 6-3 shows the dry etching rate with ECR-RIBE. For our purpose, the etching depth should be 1.5 μm - 2.0 μm, therefore we have chosen 45 seconds for our wafer.

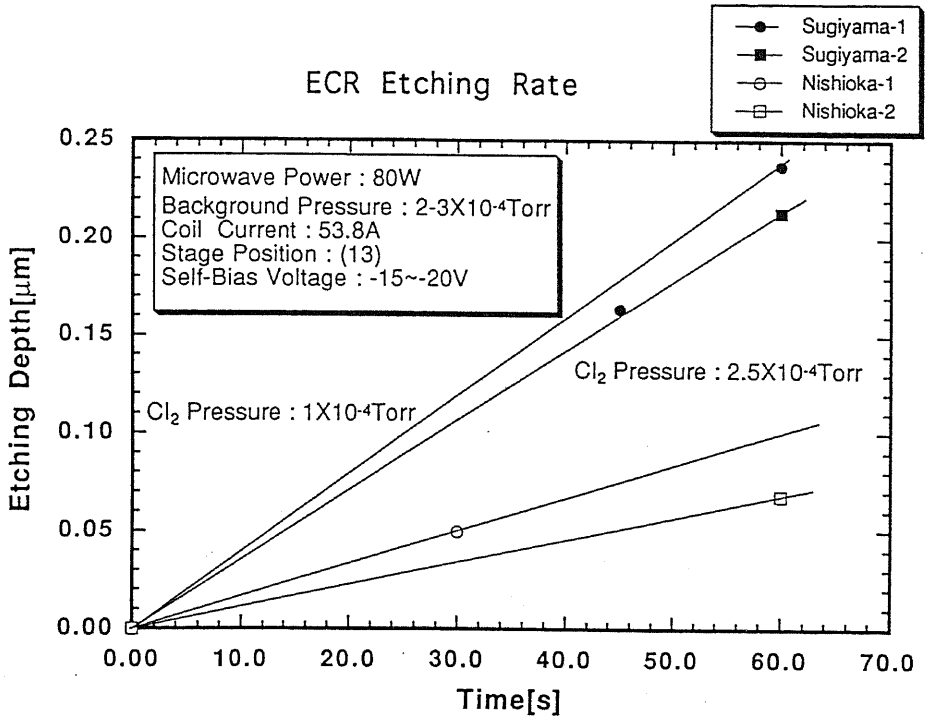

Figure 6-3 Dry etching rate of AlGaAs wafer with ECR-RIBE.

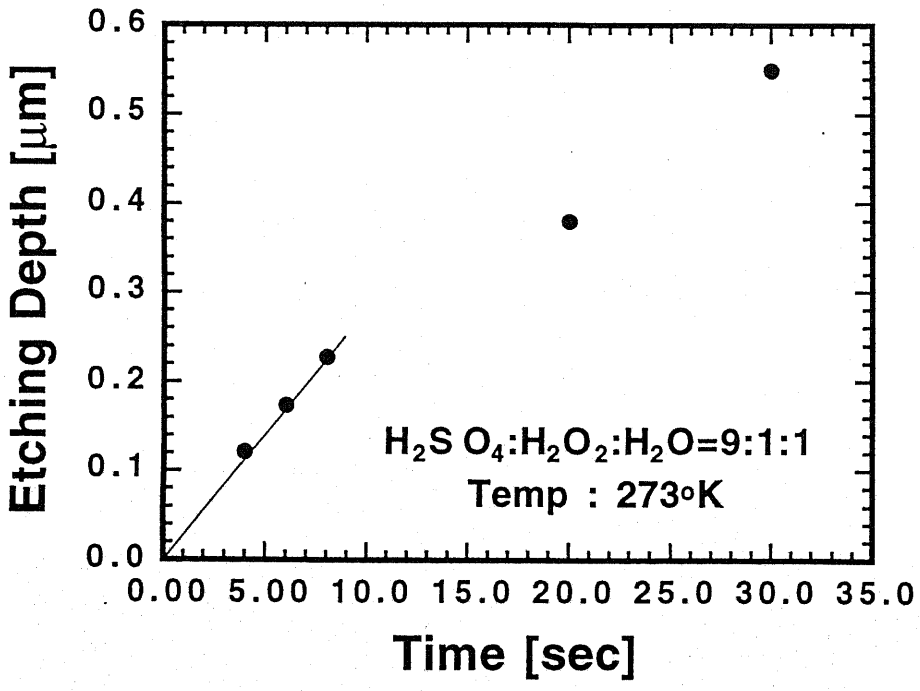

Figure 6-4 Wet etching rate of AlGaAs wafer with H_2SO_4:H_2O_2:H_2O.

After the dry etching process, the photo-resist became extremely hard, and it was difficult to remove. Then we have tried wet etching process because the wafer isn't dry any more in totally wet process. Figure 6-4 shows the wet etching rate of AlGaAs wafer with H_2SO_4:H_2O_2:H_2O= 9 : 1 : 1 . We have chosen 4 seconds to make grating.

In Figure 6-5, we show the photographs of the sampled grating on GaAs wafer. This process is done based on the two photo-lithographies in reference [6-1]. At first the photo-resist (TSMR:thinner=1:4) was spin-coated by a speed of 6000 rpm in 30 seconds, then the holographic exposure was done and baked at 135 degrees in 60 minutes. Then the second photo-resist (TSMR) was over-coated by a speed of 6000 rpm in 30 seconds, and the patterning was done by photo-rythograpy step to make long-term grating. Those two photo-resists formed the sampled grating, and the wafer was dipped in H_2SO_4:H_2O_2:H_2O= 9 : 1 : 1 in 4 seconds.

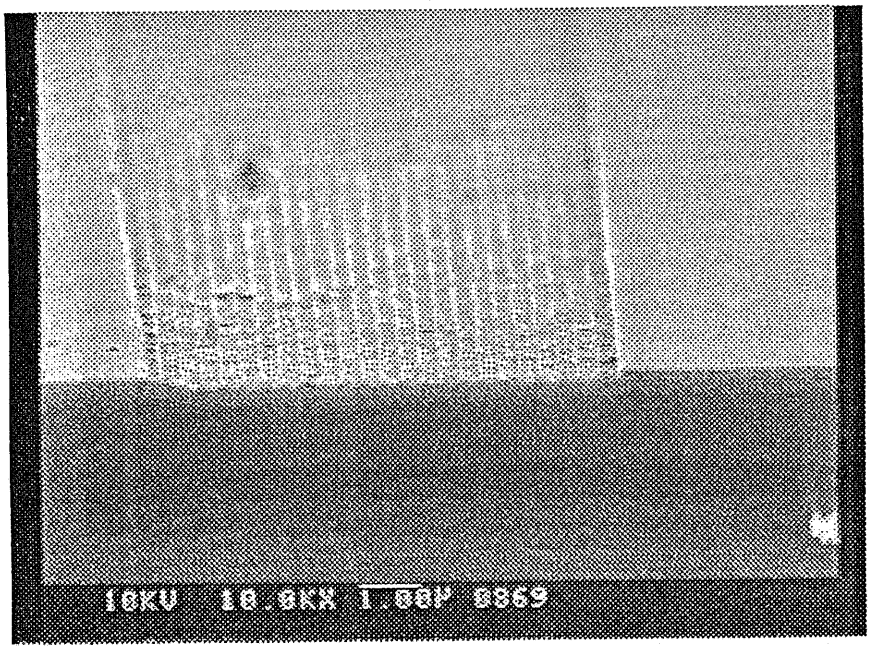

Figure 6-5 Scanning electron microscope photograph of the sampled grating.

6.4 Regrowth step

After the wet etching process, we have done the regrowth with MOCVD machine. The regrowth was successful, and the SEM photograph is shown in Figure 6-6. Here the grating period was set to be 360 nm.

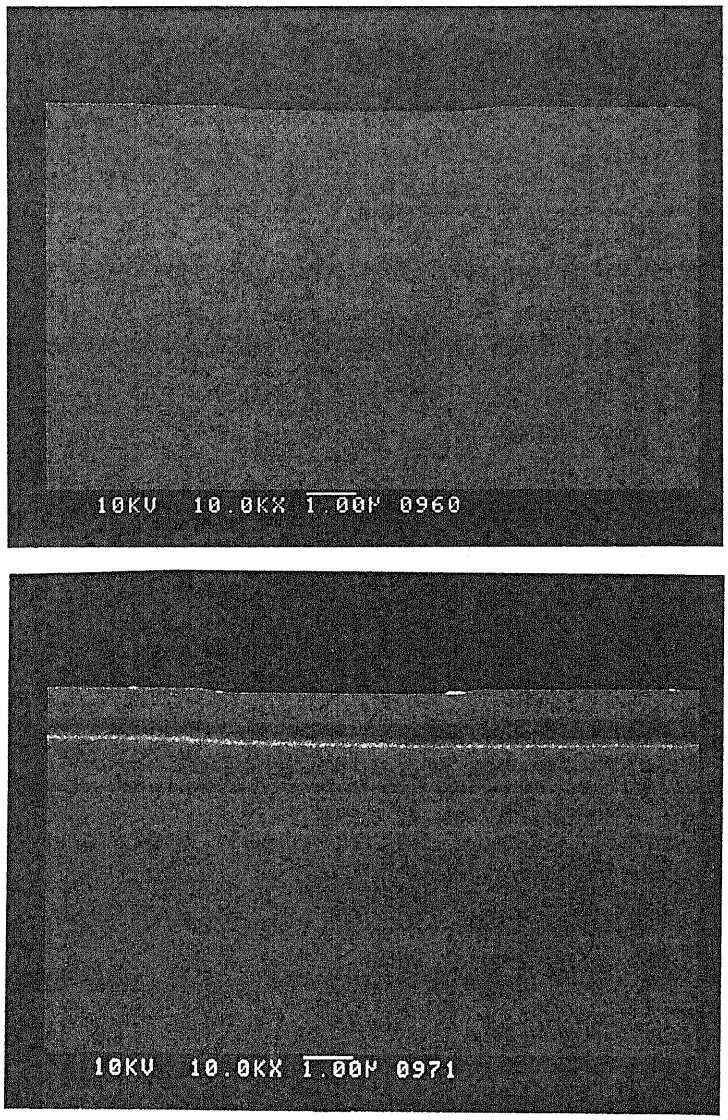

Figure 6-6 Scanning electron microscope photograph of the wafer after the regrowth. (a) with forward-coupling grating and (b) with sampled grating.

6.5 Photo-lithography step

There are six photo-lithography steps after the second epitaxy. First, a laser stripe and a mesa region were formed by wet chemical etching. After the substrate was covered by SiO2 thin film, p- and n-contact holes were etched, and gold was evaporated onto the wafer. In Figure 6-7, we show a SEM photograph of the lateral cross section of the tunable laser structure with the grating for forward-coupling. The DFBC laser, the target, will be realized if the sampled grating is substituted for the grating for forward-coupling.

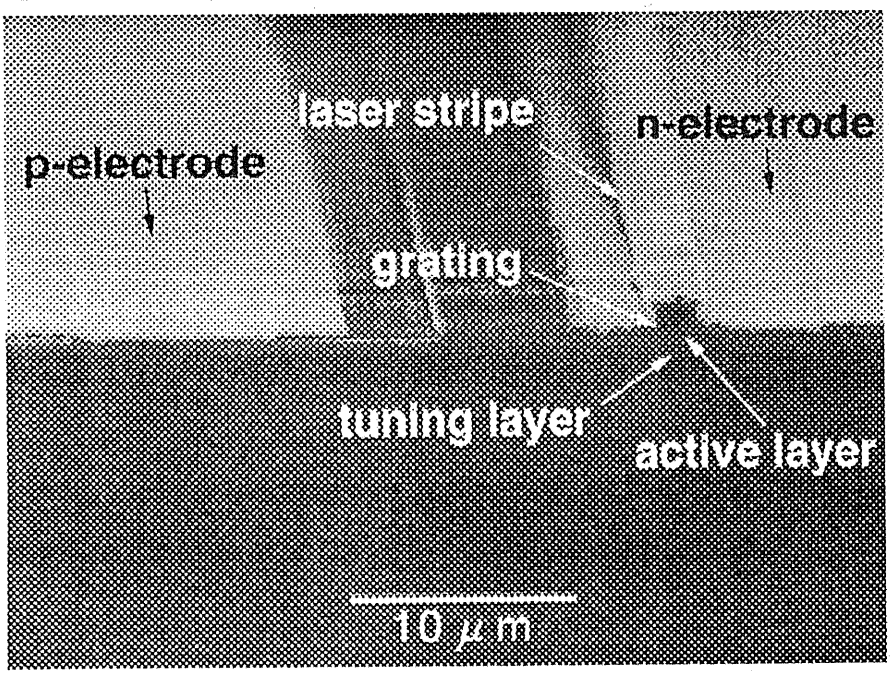

Figure 6-7 Scanning electron microscope photograph of the lateral cross section of the tunable forward-coupled laser.

In Figure 6-8, we show a SEM photograph of the DFBC laser. The backward feedback from the sampled grating is not very big, therefore both of the facets are tiltedly etched (7 degrees) by ECR-RIBE in order to reduce the facet reflection.

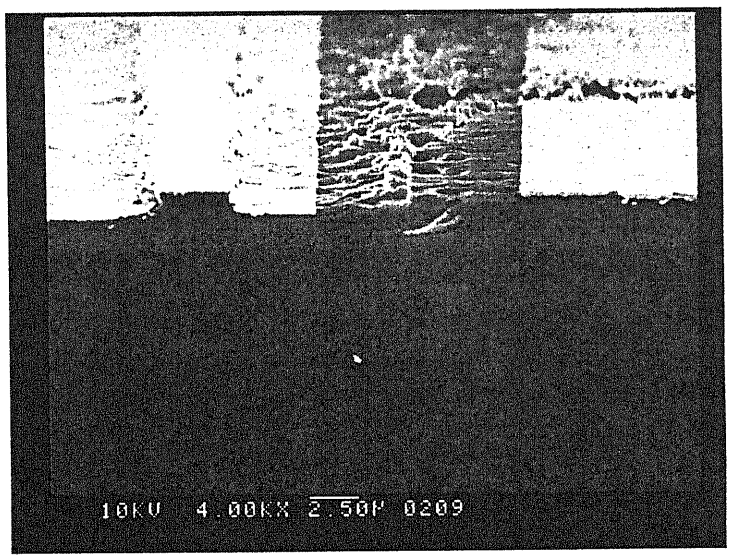

Figure 6-8 Scanning electron microscope photograph of the lateral cross section of the tunable distributed forward- and backward-coupling (DFBC) laser.

6.6 Summary

In summary, we have fabricated a tunable forward-coupled laser, and a tunable distributed forward- and backward-coupling (DFBC) laser. For the fabrication, we have measured etching-rate (both dry and wet), developed double-photo-resist technique, and the over-growth was successful.

References in Chapter 6

[6-1] T. Eguchi, "Study on Laser Triodes with three electrodes", Master's thesis, University of Tokyo, Mar. 1995.

Chapter 7 Conclusions

This dissertation described the results obtained from both a theoretical and an experimental study on widely tunable distributed forward- and backward-coupling (DFBC) lasers, comparing GC-DFBC with IC-DFBC lasers, and also describes the parameter-extraction technique (curve-fitting method) for semiconductor lasers.

We have proposed a new type of discontinuously-tunable laser, that is, distributed forward- and backward-coupling (DFBC) laser, and done a preliminary analysis by making use of the coupled-wave approach . In the DFBC laser, the main mode is selected out of distributed feedback (DFB) modes rather than the Fabry-Perot modes in DFC lasers. Therefore, larger SMSR as well as the wide range tuning of the discontinuously-tunable lasers are expected. In this theory we have done a preliminary experiment, i.e., fabrication of a proto-type of DFBC lasers.

In Chapter 2, we have described a new tunable laser diode, i.e., the distributed forward- and backward-coupling (DFBC) laser. This laser is characterized by a codirectional forward coupling between two parallel waveguides together with a backward distributed Bragg feedback due to sampled grating. It would provide a wide tuning range (over 40 nm, for example) as well as larger SMSR in principle compared with the other types of discontinuously-tunable laser diodes. Simple one current tuning scheme is another advantage of the DFBC laser. Either gain or index coupling, or a combination of these may be used with the DFBC laser. However, the gain coupling is preferable as it could lead to larger SMSR.

In Chapter 3, we have shown some simulation results based on two different thories. This laser is a combination of a codirectional forward coupling between two parallel waveguides together with a backward distributed Bragg feedback due to sampled grating. The filter characteristics are extremely sensitive to

the change of the refractive index of one of the waveguides. The tuning range would easily be as wide as 40 nm which is used in erbium-doped fiber amplifier (EDFA) bandwidth. We have proposed two different approaches to analyze this kind of laser, coupled-mode analyais and mode-expansion method. The mode-expansion analysis is more rigorous than the coupled-mode analysis. However, in both analyses the tuning range would be about 40 nm when the refractive index change is as little as 0.01 of one of the waveguide. Basically the former approach would be closer to the latter method when the duty cycle of the sampled grating is very small. In our simulation, the duty cycle was less than 5 %. That is why both two analyses have shown the similar results.

In Chapter 4, excellent agreement between theoretical and experimental spectra is obtained in spite of the possible non-uniformities in the devices and in spite of the rough approximations for gain and spontaneous emission. In some cases, a better agreement could probably be reached if we used a wavelength dependent spontaneous emission rate and/or a wavelength dependence of the gain that is more suited for quantum wells than the parabolic function used here. In order to apply this method for DFBC lasers, one should impliment multi-section and multi-mode analysis. This is a futher investigation of this study.

In Chapter 5, we describe the four steps of the structure design. This particular device needs only one regrowth step, however needs eight photo-masks. The distance between the p-electrode and the n-electrode is designed to be 20 μm in order to make the process tolerance high. For this design, the refractive index change in the tuning layer is still big and the tuning range would be 4 nm for 0.84 μm wavelength scheme. Our photo-masks are designed in order to simplify the process steps, however we need still eight masks. Each step is designed for higher process tolerance such as 5 μm error.

In Chapter 6, we have fabricated a tunable forward-coupled laser and a

tunable distributed forward- and backward-coupling laser. For the fabrication, we have measured etching-rate (both dry and wet), developed double-photo-resist technique, and the over-growth was successful.

Publications

Journals and Letters

[1] K. Sato, Y. Nakano, and K. Tada, "Wavelength tuning characteristics of widely tunable distributed forward- and backward-coupling semiconductor laser", IEEE Photon. Technol. Lett., pp. 257-259, Mar. 1995.

International Conferences

[2] G. Morthier, R. Fujitani, K. Sato, R. Baets, Y. Nakano, and K. Tada, "Enhanced Performance of DFB Lasers for Analog Communication Systems by the Introduction of Gain Coupling", submitted to First Optoelectronics and Communications Conference (OECC'96), Makuhari, Chiba, 1996.

[3] K. Sato, Y. Nakano, and K. Tada, "Distributed forward- and backward-coupling laser", Technical Digest, Topical Meeting on Photonics in Switching (PS'95), PFB7, pp. 141-143, Salt Lake City, Mar. 1995.

[4] G. Morthier, K. Sato, R. Baets, T. K. Sudoh, Y. Nakano, and K. Tada, "Parameter extraction from subthreshold spectra in cleaved gain- and index-coupled distributed feedback laser diodes", Conference on Optical Fiber Communication (OFC'95), FC3, San Diego, Mar. 1995.

[5] J. Buus, D. J. Robins, J. Haes, K. Sato, and R. Baets, "Asymmetric spot size expander for improved waveguide to fiber coupling", Topical Meeting on Integrated Photonics Research (IPR'94), ThF17-1, San Francisco, California, Feb. 1994.

[6] K. Sato, G. Morthier, R. Baets, Y. Nakano, and K. Tada, "Optimum design of the grating for gain/loss coupled DFB lasers", 19th European Conference on Optical Communication (ECOC'93), Tu 10, Montreux, Switzerland, Sept. 1993.

Workshops

[7] K. Sato, G. Morthier, and R. Baets, "Simulation of short optical pulse generation in gain-coupled DFB semiconductor lasers", 1993 European Semiconductor Laser Workshop, Session 1-6, Rigi-Kaltbad, Switzerland, Sept. 1993.

国内大会論文

[8] 佐藤健二、二口尚樹、中野義昭、多田邦雄、「波長可変方向性結合レーザの作製 － DFBC レーザの実現へ向けて」、第４３回応用物理学会関係連合講演会、東洋大学、1996 年 3 月、にて発表予定。

[9] 名倉徹、佐藤健二、G. モルティエル、R. バーツ、中野義昭、多田邦雄、「DFB レーザの閾値下スペクトルからのパラメータ抽出 (II)」、第４３回応用物理学会関係連合講演会、東洋大学、1996 年 3 月、にて発表予定。

[10] 藤谷龍一郎、佐藤健二、G. モルティエル、R. バーツ、中野義昭、多田邦雄、「増幅性格子利得結合 DFB レーザの三次高調波歪み解析」、第４３回応用物理学会関係連合講演会、東洋大学、1996 年 3 月、にて発表予定。

[11] 李錫、川西秀和、佐藤健二、中野義昭、多田邦雄、「EA 変調器集積化 3 セクション波長可変 DBR レーザの静特性解析」、第５６回応用物理学会学術講演会、28a-SQ-25、金沢工業大学、1995 年 8 月。

[12] 佐藤健二、中野義昭、多田邦雄、「分布並進逆進結合半導体レーザのモード展開法による解析」、第４２回応用物理学会関係連合講演会、30a-ZG-2、東海大学、1995年3月。

[13] 佐藤健二、G. モルティエル、R. バーツ、須藤剣、中野義昭、多田邦雄、「利得/屈折率結合DFBレーザの閾値下スペクトラムからのパラメータ抽出」、第４２回応用物理学会関係連合講演会、30a-ZG-4、東海大学、1995年3月。

[14] 佐藤健二、中野義昭、多田邦雄、「広帯域波長可変な分布並進逆進結合半導体レーザの波長可変シミュレーション」、第５５回応用物理学会学術講演会、22a-S-8、名城大学、1994年9月。

[15] 佐藤健二、G. モルティエル、R. バーツ、中野義昭、多田邦雄、「半導体利得結合DFBレーザにおける光短パルス発生のシミュレーション」、第５４回応用物理学会学術講演会、27p-H-11、北海道大学、1993年9月。

[16] 佐藤健二、G. モルティエル、R. バーツ、中野義昭、多田邦雄、「増幅性格子利得結合分布帰還型半導体レーザの小信号応答特性」、第４０回応用物理学会関係連合講演会、30p-C-4、青山学院大学、1993年3月。

[17] D. K. ゴータム、佐藤健二、中野義昭、多田邦雄、「GaAsへの低濃度Cd拡散」、第３８回応用物理学会関係連合講演会、30p-K-10、東海大学、1991年3月。

[18] D. K. ゴータム、佐藤健二、中野義昭、多田邦雄、「バイポーラトランジスタ構造導波路型光スイッチ作製に向けた開管法二重拡散」、第３８回応用物理学会関係連合講演会、30p-K-11、東海大学、1991年3月。

Acknowlegement

At first I'd like to thank the deepest gratitude to my research advisor professor Dr. Kunio TADA for his guidance and encouragement. I'm also grateful to Prof. Dr. Yoshiaki NAKANO for his constant supervising.

My special thanks are due to Prof. Dr. Roel BAETS and Dr. Geert MORTHIER of Gent University for their great and kind help during my stay in Belgium. The discussion with them extremely helped me to study this subject. I would also like to thank Mr. Piet VERHOEVE for his help of measuring spectra of DFB lasers.

I would like to thank Prof. M.-C. Amann of Kassel University for helpful suggestions and advice.

Acknowledgements are also due to Prof. Dr. Yi Luo of Tsinghua University for a great discussion.

I greatly appreciate Mr. Shinji IIO of Yokogawa Electroc Corporation for our epitaxiall growth, and my thanks also go to Mr. Tsurugi K. SUDOH of Nakano Laboratory.

I'd like to thank Mr. Toru MURAI for his help in various aspects. Dr. Yukihiro SHIMOGAKI and Mr. Masakazu SUGIYAMA of Komiyama Laboratory helped me for dry-etching, and Tomoaki TODA gave me a very important suggestion for a general fabrication process and a help for liquid phase epitaxy. Other people of Tada/Nakano Laboratories also helped me a lot during my doctrate course.

At last I wish to express my special thanks to Mr. Naoki FUTAKUCHI for his kind help of doing hard experiments.